HUGHES RESEARCH LABORATORIES
Malibu, California

a division of hughes aircraft company

HIGH-TEMPERATURE LIQUID-MERCURY CATHODES FOR ION THRUSTERS

Quarterly Progress Report No. 3
1 December 1966 through 28 February 1967
Contract No. NASW-1404

K. W. Arnold, W. O. Eckhardt, G. Hagen,
J. A. Snyder, and R. C. Knechtli
Plasma Physics Department

TABLE OF CONTENTS

LIST OF ILLUSTRATIONS

I. INTRODUCTION AND SUMMARY

This report is concerned with the continued development of liquid mercury cathodes for use in Kaufman-type thrusters which have high shell temperatures, as in a clustered array. Earlier papers and reports have described both the cathode* and its satisfactory operation under an extended life test in a thruster**.

Thermal design analysis for the high temperature liquid mercury cathode has now been extended to include rejection of heat from the thruster shell, and is contained in Section II. Starting from first principles, the relationships between various cathode parameters are derived, and the thermal resistance of the cathode between the pool and the thermocouple location is calculated for both circular and annular pool geometries. The substantially lower thermal resistance for the latter case is clearly shown. The variation of the cathode temperature drop with beam current has also been considered, and even with a low beam current the advantages of annular over circular geometry are plainly demonstrated.

Heat rejection from the cathode to the thruster shell by conduction through the thruster end plate has been estimated for a number of geometries, so that a particular configuration combining good heat conduction with low weight can be chosen. If this is done for a 20-cm diameter thruster, it is shown that for an overall weight of about 8 lb.†, the shell can operate at 175°C

---

* W. O. Eckhardt, J. A. Snyder, H. J. King, and R. C. Knechtli, "A New Cathode for Mercury Electron-bombardment Thrusters," AIAA Paper No. 64-690 (August 1964).
H. J. King, W. O. Eckhardt, J. W. Ward, and R. C. Knechtli, "Electron-Bombardment Thrusters using Liquid-Mercury Cathodes," AIAA Paper No. 66-232 (March 1966).

** W. O. Eckhardt, H. J. King, J. A. Snyder, J. W. Ward, W. D. Myers, and R. C. Knechtli, "4,000-hr Life Test of a Liquid-Mercury Cathode in a 20-cm LeRC Ion Thruster," Hughes Research Laboratories Special Report for Contract NAS 3-6262 (Nov. 1966).

† This applies to a thruster with 600 mA beam current and $K_e/K_a = 12$. At a specific impulse of 4000 sec, $\eta_m = 90\%$ and a thruster power efficiency of 82% (450 eV/ion), the corresponding weight to power ratio would be 5.3 lb./kW.

with the thruster in a peripheral array, and that the corresponding cathode temperature is 300°C. Satisfactory operation of LM cathodes at this and higher temperatures has already been demonstrated both in diode and thruster configuration.

Section IIIA begins with the derivation of a normalized performance parameter, so that meaningful comparisons of cathode performance between different cathodes or between modifications can be made. Following a description of the cathode modifications which were made, an account is given of a new operating mode for LM cathodes, using mercury vapor rather than liquid mercury feeding. It is shown that the diffuse spot-pattern mode which results is not the same as modes described in earlier literature, and is probably due to transient condensation of vapor on the walls of the pool keeping structure. This novel cathode mode promises several advantages over liquid-fed cathodes, including higher thruster efficiency, lower thermal loading of the cathode, the use of the same feed system and isolator as other thrusters presently use, and even the possibility of only feeding a fraction of the propellant through the cathode.

Test results for the vapor-fed cathode are included in a table, analyzing results for all cathode modifications and including the normalized parameter described above. The evolution of high-temperature LM cathode designs can now be evaluated: for example it is evident that Cathode No. 25-II and Cathode No. 26-III can meet and exceed all requirements for 15 cm and 20 cm thruster use respectively.

Section IIIB describes work performed this quarter on an LM neutralizer cathode. Replacement of a mechanical by an electrical igniter showed that in earlier experiments the predominant mercury loss was, as speculated, by igniter splashing rather than by evaporation. As a consequence stable LM cathode operation in the neutralizer current range was demonstrated at good electron-to-atom emission ratios (> 50) for periods up to several hours, at temperatures close to the equilibrium value at which cooling occurs by radiation from the neutralizer face.

Sections IVA & B relate to experiments performed with Cathode No. 25-II in the 15-cm, permanent magnet configuration thruster. Use of a four-aperture, variable baffle showed that optimum thruster performance was given by the smallest annular aperture tried, having an open area of only 0.28 cm^2. This configuration was subsequently tested during a 4 hour run,

giving a beam current of 440 mA at a source energy per ion of 417 eV/ion and 82% mass utilization.

In a subsequent series of experiments, a probing baffle carrying both a small pinhole and a narrow slot was used to investigate the contribution per unit area of the cathode vapor cone region to the formation of ions in the discharge chamber. Both probing geometries showed that the segment of the 30° half angle vapor cone along its boundary has the greatest effect on the beam current, and that if the pinhole (or other aperture) is moved outside of the vapor cone region a rapid decrease in beam current occurs. These results can be explained in terms of the escape of electrons from the vapor region, rather than the change in efflux of any significant quantity of mercury vapor through the small apertures used.

The significance of these findings is that they point out the possibility of affecting relatively independently the admission of electrons and neutral atoms into the discharge chamber, using improved versions of our discharge chamber baffles. This should lead to further substantial increases in thruster efficiency.

II. ANALYSIS OF THERMAL DESIGN REQUIREMENTS

A. -Introduction

Operation of the LM cathode at high temperatures (250° to 300°C) is achieved by shrinking the exposed mercury surface to a small size in order to reduce the evaporation of mercury and to keep the electron-to-atom ratio at the cathode, K_e/K_a, at the desired level (from 10 to 20). The thermal design requirements for the high-temperature LM cathode were considered in an earlier report*, where the advantages of annular over circular cathode geometry in heat conduction for the mercury pool were clearly demonstrated. The analysis contained here is somewhat more comprehensive, and includes rejection of heat from the thruster shell.

B. -Cathode Parameters

This analysis will consider only circular and annular LM cathode geometries, although it is expected that the thermal properties of a high temperature rectangular slit cathode would be similar to those of an annular cathode. The circular cathode is shown in Fig. 1, while Fig. 2 is a scale drawing (20:1) of an annular cathode, with mean annular radius $\bar{r}$ and width of exposed mercury surface Δr. Other parameters are the beam current I_B; the mass utilization η_m; the cathode current I_K; the flux density L_a of the evaporating mercury atoms; the area of the exposed mercury surface A_K at the cathode; the temperature of the mercury T_{Hg}; the heat conductivity k_{th} of the cathode material; and the ratio $V_{K,th}$ of the thermal power delivered to the cathode, $P_{K,th}$, to the cathode current, I_K.

Assuming that evaporation is the predominant loss of mercury from the cathode, and that back scattering can be neglected, then

$$L_a = \frac{1}{4} n \bar{c} ,$$

where n is the equilibrium number density in saturated mercury vapor equivalent to temperature T_{Hg} and $\bar{c}$ is the mean vapor velocity. As a consequence,

---

* Quarterly Progress Report #1, Contract #NASW-1404 (1 June 1966 through 31 August 1966).

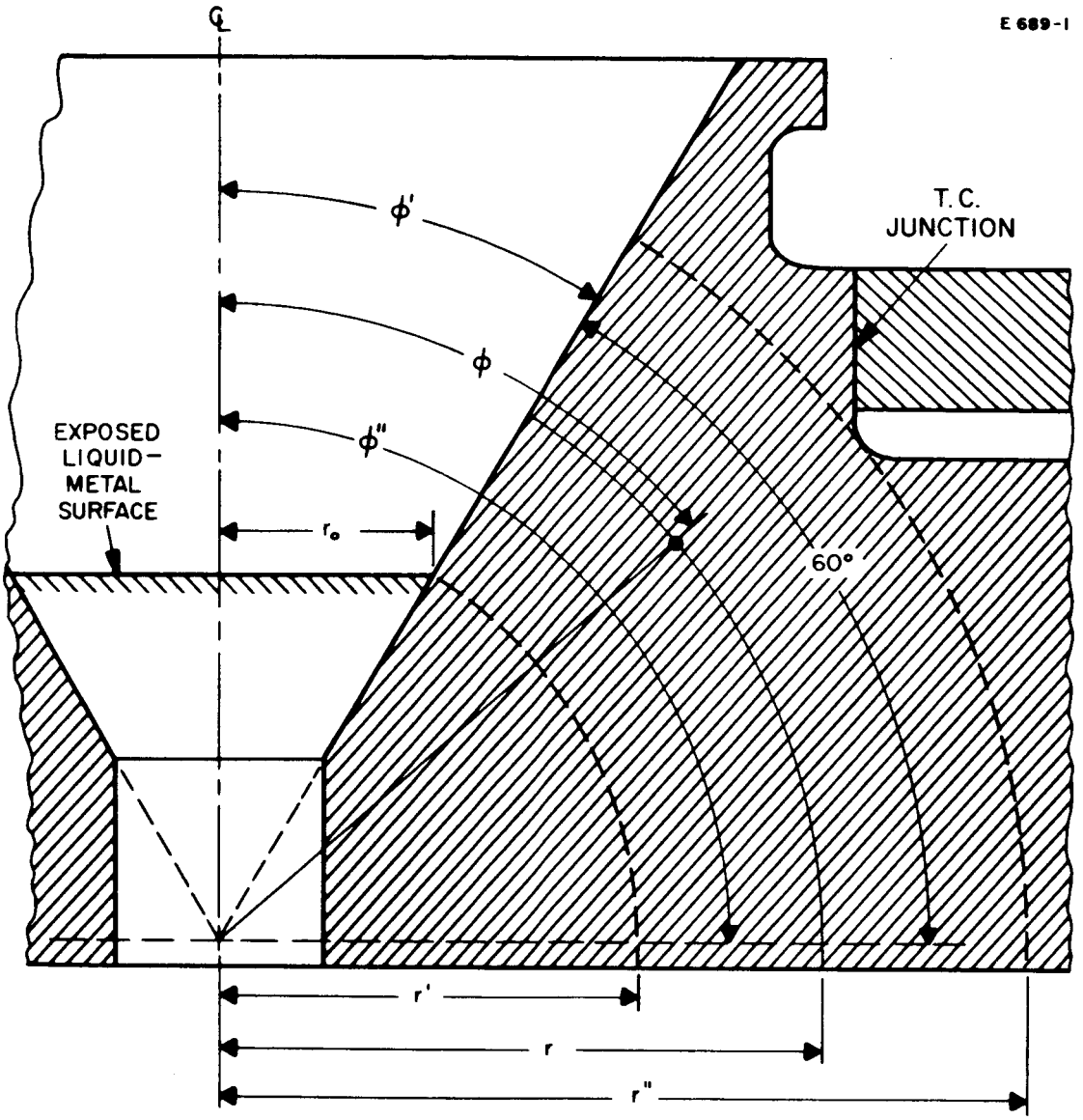

Fig. 1. Schematic cross section of circular LM cathode design (not to scale).

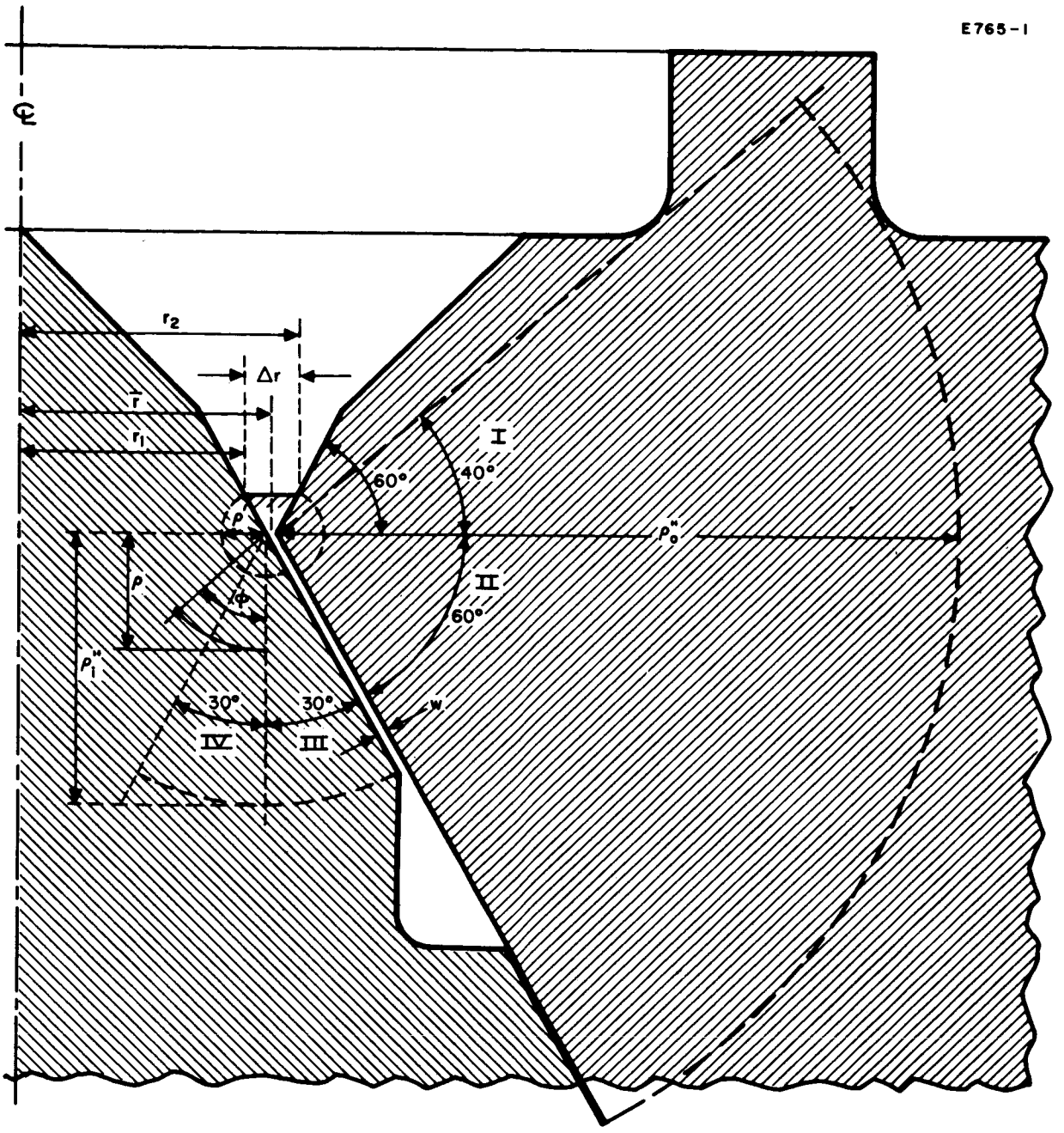

Fig. 2. Schematic cross section of annular LM cathode design (not to scale).

we also have

$$L_a = \frac{p_{Hg}(T_{Hg})}{(2\pi m_{Hg}\, kT_{Hg})^{1/2}} ,$$

where $p_{Hg}(T_{Hg})$ is the saturated vapor pressure of mercury, m_{Hg} is the atomic mass of Hg, and k is Boltzmann's constant.

The total number of atoms evaporated per second is then

$$K_a = L_a A_K$$

$$= \frac{\pi r^2 p_{Hg}}{(2\pi m_{Hg}\, kT_{Hg})^{1/2}} \quad \text{for the circular cathode}$$

and

$$K_a = \frac{2\pi \bar{r}\, \Delta r\, p_{Hg}}{(2\pi m_{Hg}\, kT_{Hg})^{1/2}} \quad \text{for the annular cathode,}$$

where e is the electronic charge.

Fig. 3 shows p_{Hg}, L_a and the ratio I_B/A_K as functions of T_{Hg}, the latter for values of η_m = 100, 90 and 80%.

The range of T_{Hg} between 200 and 350°C (473° to 623°K) is particularly interesting. In Fig. 4 the relationship

$$A_K = I_K/(e\, L_a\, K_e/K_a)$$

is plotted for various temperatures T_{Hg} and values of the electron-to-atom emission ratio K_e/K_a. For example with I_B = 0.250A, η_m = 85% and T_{Hg} = 300°C, $A_K = 7.5 \times 10^{-5}$ cm^2 and I_K = 3.16A with K_e/K_a = 10.

C. -Cathode Temperature Measurements

Because of the small area of the mercury surface and the relatively low thermal conductivity of mercury (about 10 times less than molybdenum) it is not possible to measure the mercury temperature directly with a thermocouple. Instead the junction has been placed a short distance away from the pool and the temperature difference $T_{Hg} - T_K$ was estimated. This was done in the case of the circular cathode by assuming concentric spherical isotherms (Fig. 1) between the mercury pool and the thermocouple junction. As the radius of the mercury pool is enlarged, the effective thermal resistance between the

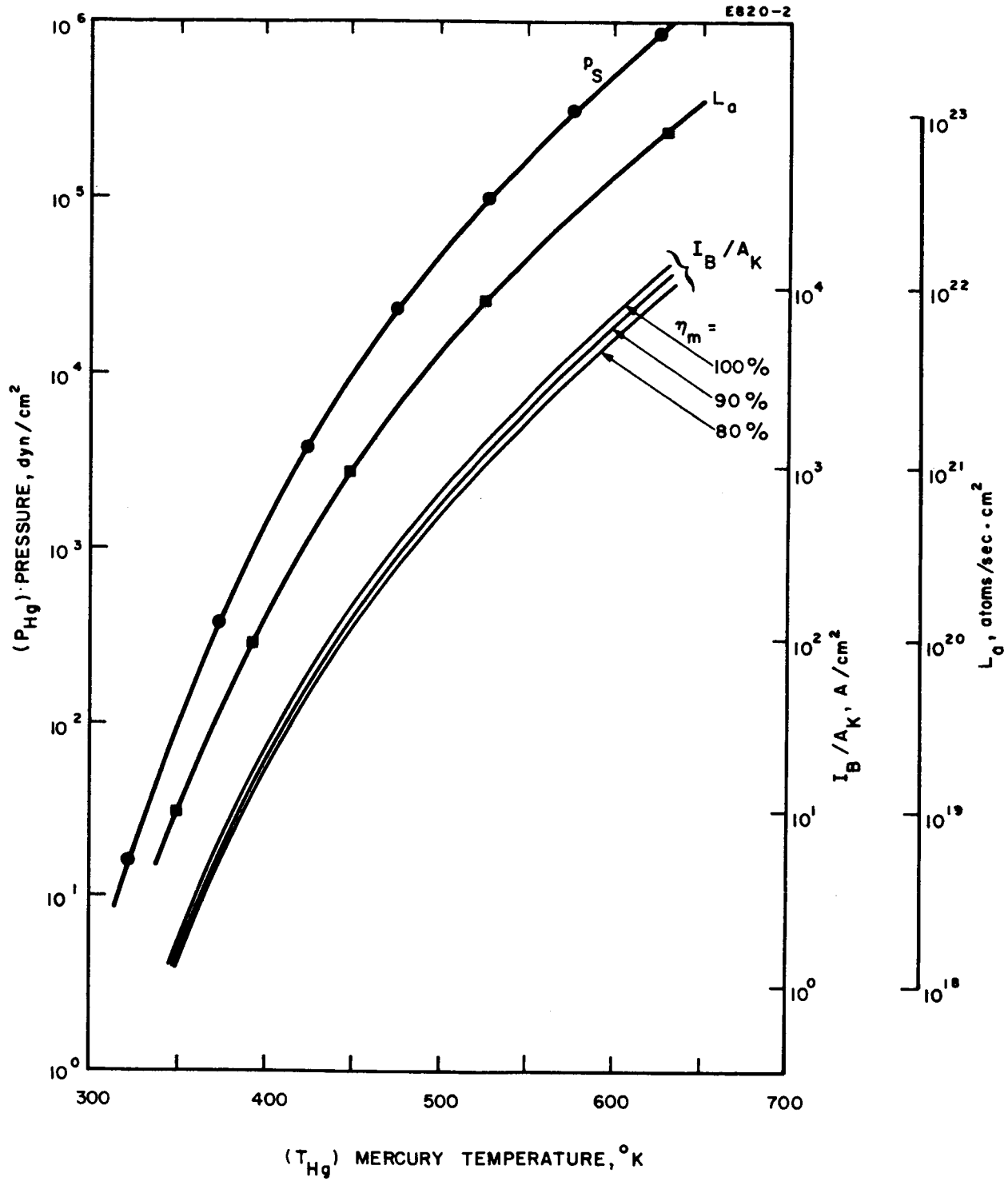

Fig. 3. Saturated vapor pressure p_{Hg}, evaporation rate and ratio I_B/A_k as a function of mercury temperature.

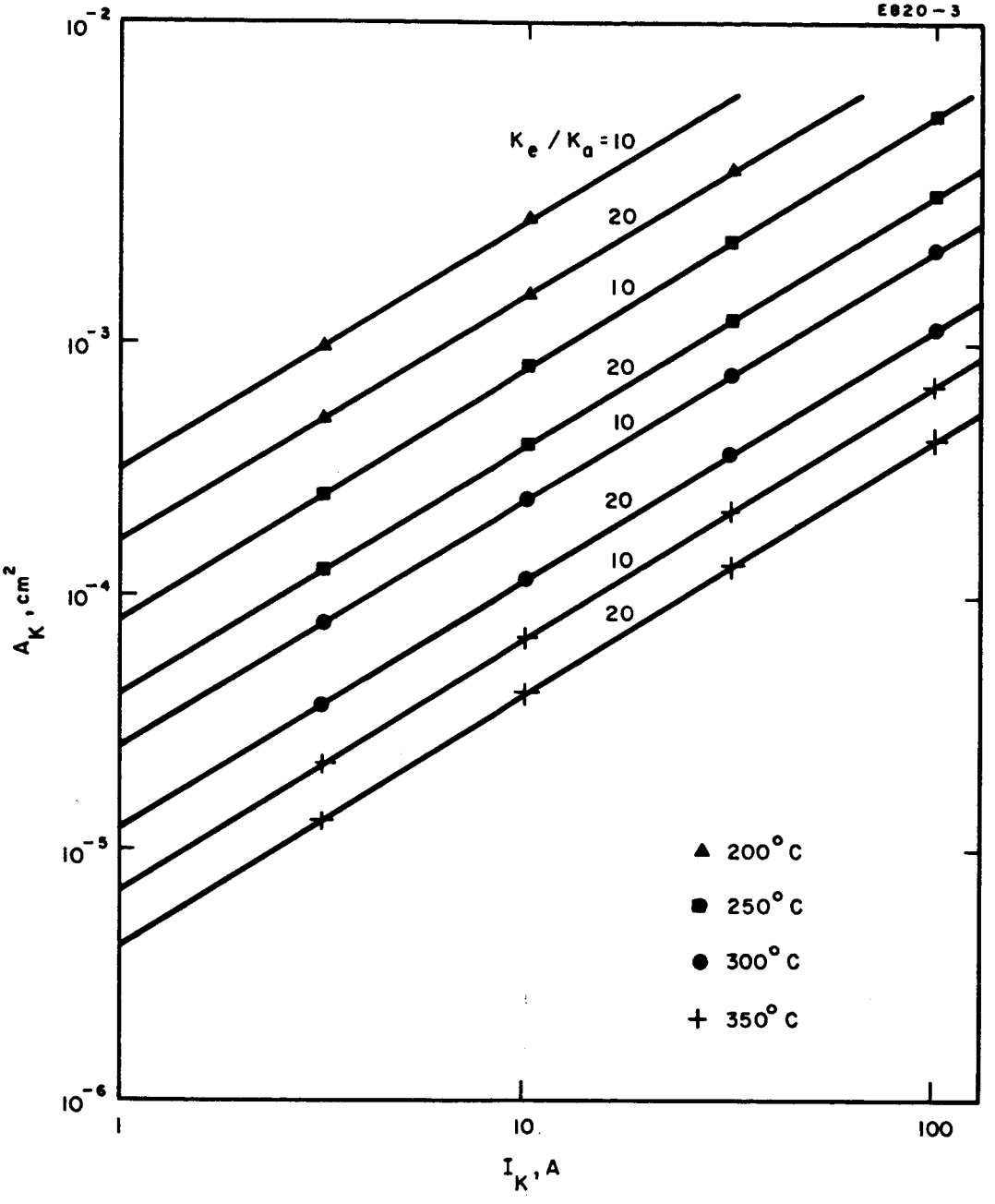

Fig. 4. A_K as a function of I_K for various T_{Hg} and K_e/K_a values.

pool and an isotherm through the thermocouple decreases in the manner shown in Fig. 5.

In the annular case concentric toroidal isotherms were assumed (Fig. 2). Now the thermal resistance R_{th} between two toroidal isotherms of major radius $\bar{r}$ and minor radii ρ' and ρ'' is

$$R_{th} = \frac{1}{2\pi k_{th} b} \ln \frac{\rho''(c\rho' + b)}{\rho'(c\rho'' + b)}$$

where $b = \bar{r}(\Phi''-\Phi')$ and $c = \cos \Phi' - \cos \Phi''$. In the figure ρ' is also equal to Δr.

Dividing the cathode environs into region I to IV as shown on Fig. 2, the effective resistance becomes

$$R_{th,eff} \simeq \frac{1}{\sum_n \frac{1}{R_{th}^n}} .$$

Because $\bar{r} \gg \Delta r$,

$$R_{th} \simeq \frac{1}{2\pi k_{th} b} \ln \frac{\rho'' b}{\Delta r (c\rho'' + b)} .$$

Figures 6 through 10 show the relationship between A_K and R_{th} for n = I to IV, as well as the effective value for R_{th}. In zones I and II, ρ'' was taken as 0.25 cm, while in zones III and IV as 0.075 cm. As $\bar{r}$ is lowered from 0.21 to 0.15 cm the value of R_{th} for a particular A_K increases. In order to minimize the temperature drop between the mercury pool and the radiating surface, a low value for R_{th} is needed, leading to a large value for $\bar{r}$. In practice $\bar{r}$ is limited by the dimension Δr, which cannot conveniently be less than about 5×10^{-4} cm. In Fig. 2, $\bar{r} = 0.19$ cm, giving $\Delta r = 5 \times 10^{-4}$ cm for $A_K = 6 \times 10^{-4}$ cm^2.

To compare the two geometries, consider a cathode operating at $T_{Hg} = 250^{\circ}C$, with an $I_B = 500$ mA at $\eta_m = 90\%$; then from Fig. 4, $A_K = 4.2 \times 10^{-4}$ cm^2, and with $K_e/K_a = 12$, $I_K = 6.5$A. From Fig. 5 the effective thermal resistance for the circular cathode which corresponds to this A_K is $5.5^{\circ}K\ W^{-1}$, while from Fig. 10 for a representative annular cathode ($\bar{r} = 0.19$ cm) it is $1.3^{\circ}K\ W^{-1}$. Assuming a value for $V_{K,th}$ of $2.5\ WA^{-1}$ the temperature difference between the mercury pool and the thermocouple, 0.44 cm away from the center line of the cathode, is $89^{\circ}C$ for the circular and $21^{\circ}C$ for the annular cathode.

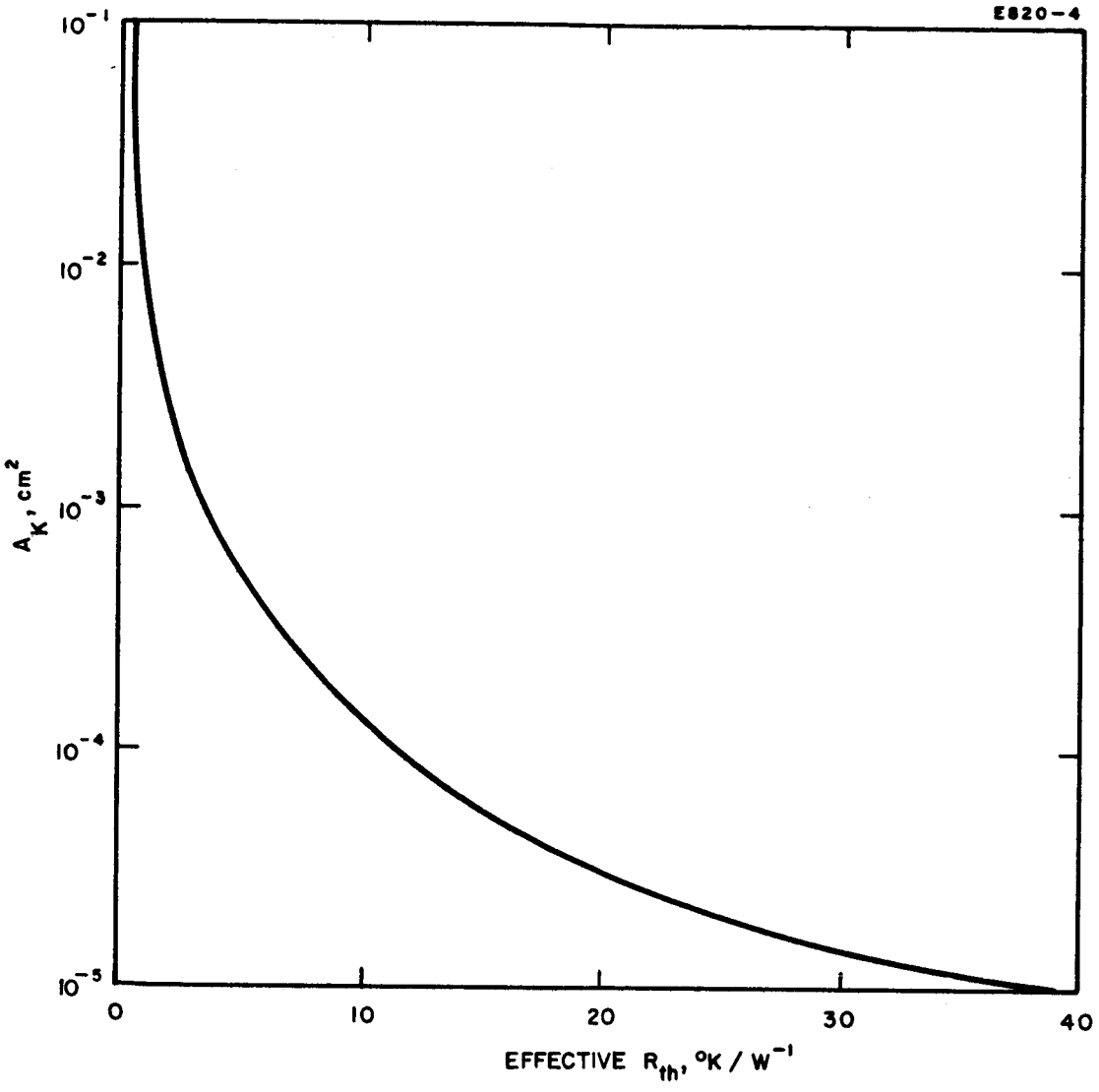

Fig. 5. Effective cathode thermal resistance as a function of mercury surface area (circular geometry).

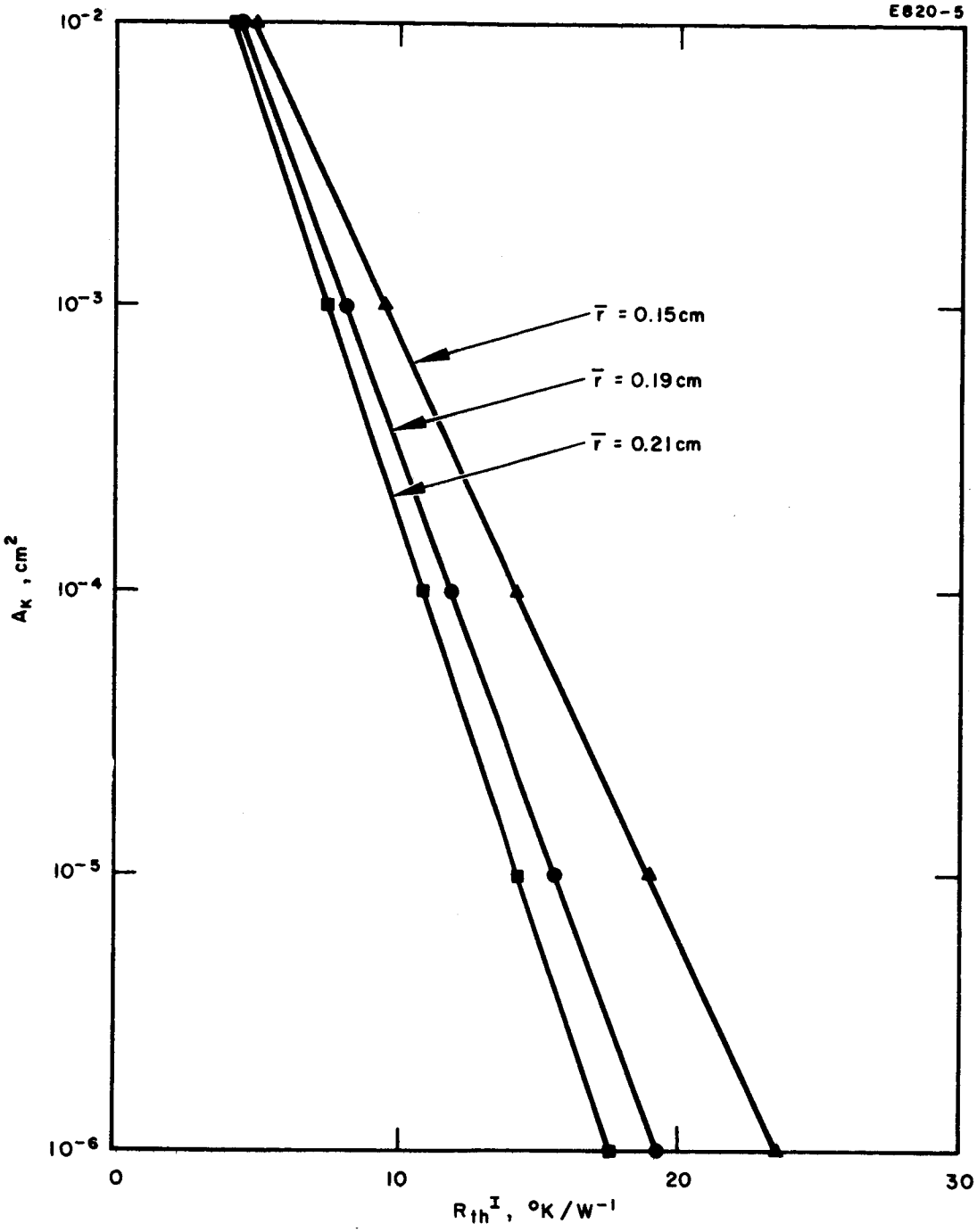

Fig. 6. Thermal resistance in cathode region I as a function of mercury surface area.

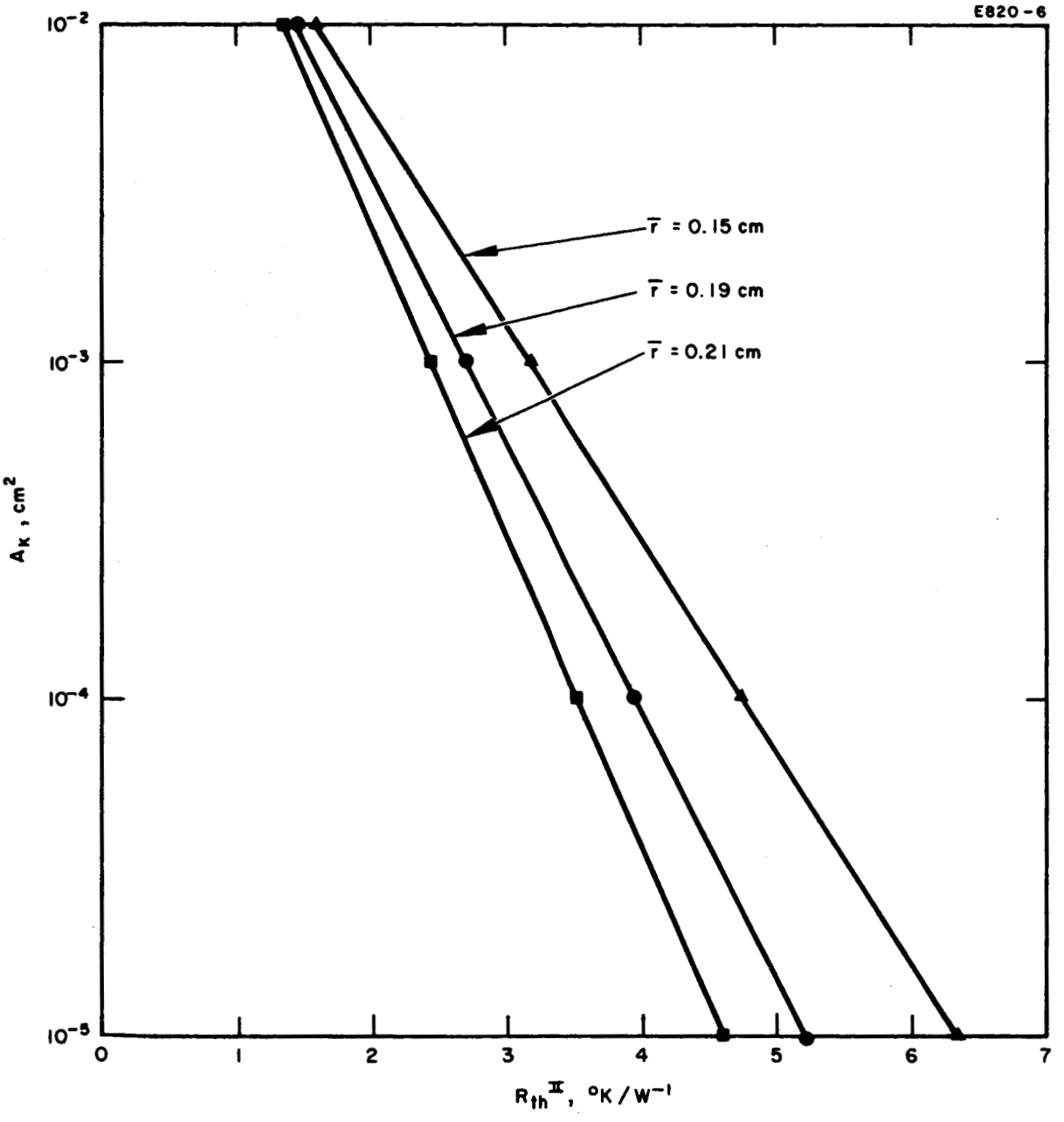

Fig. 7. Thermal resistance in cathode region II as a function of mercury surface area.

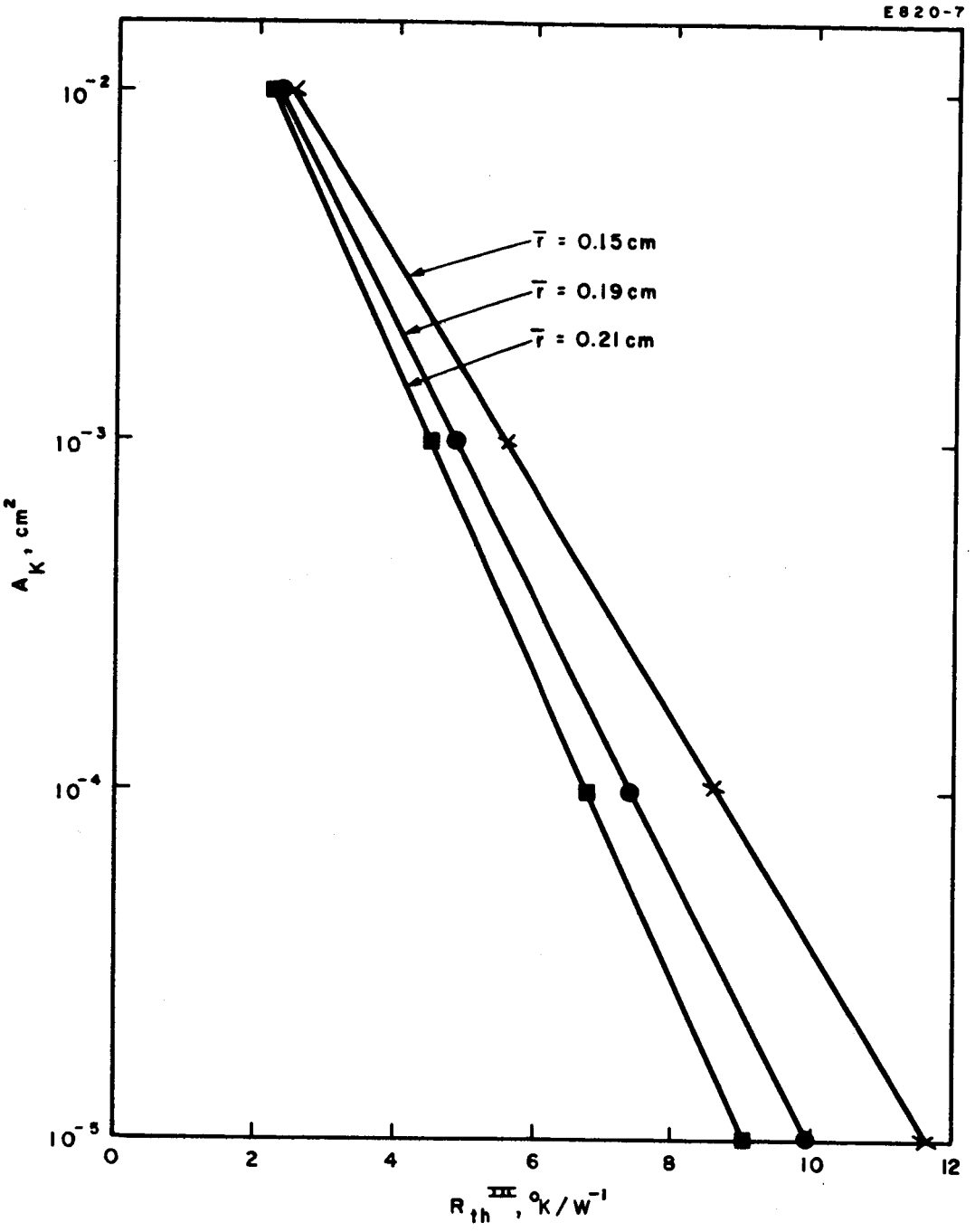

Fig. 8. Thermal resistance in cathode region III as a function of mercury surface area.

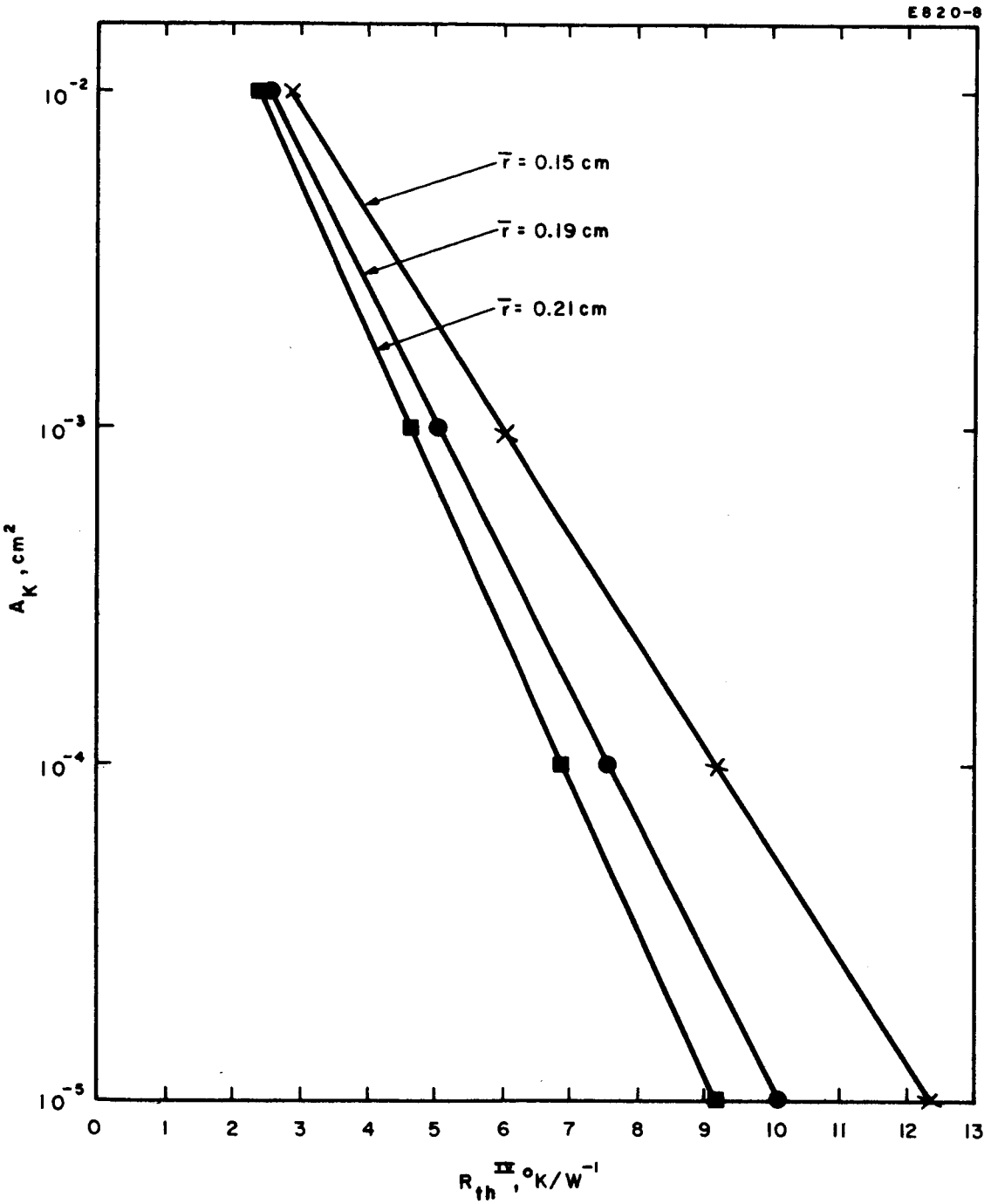

Fig. 9. Thermal resistance in cathode region IV as a function of mercury surface area.

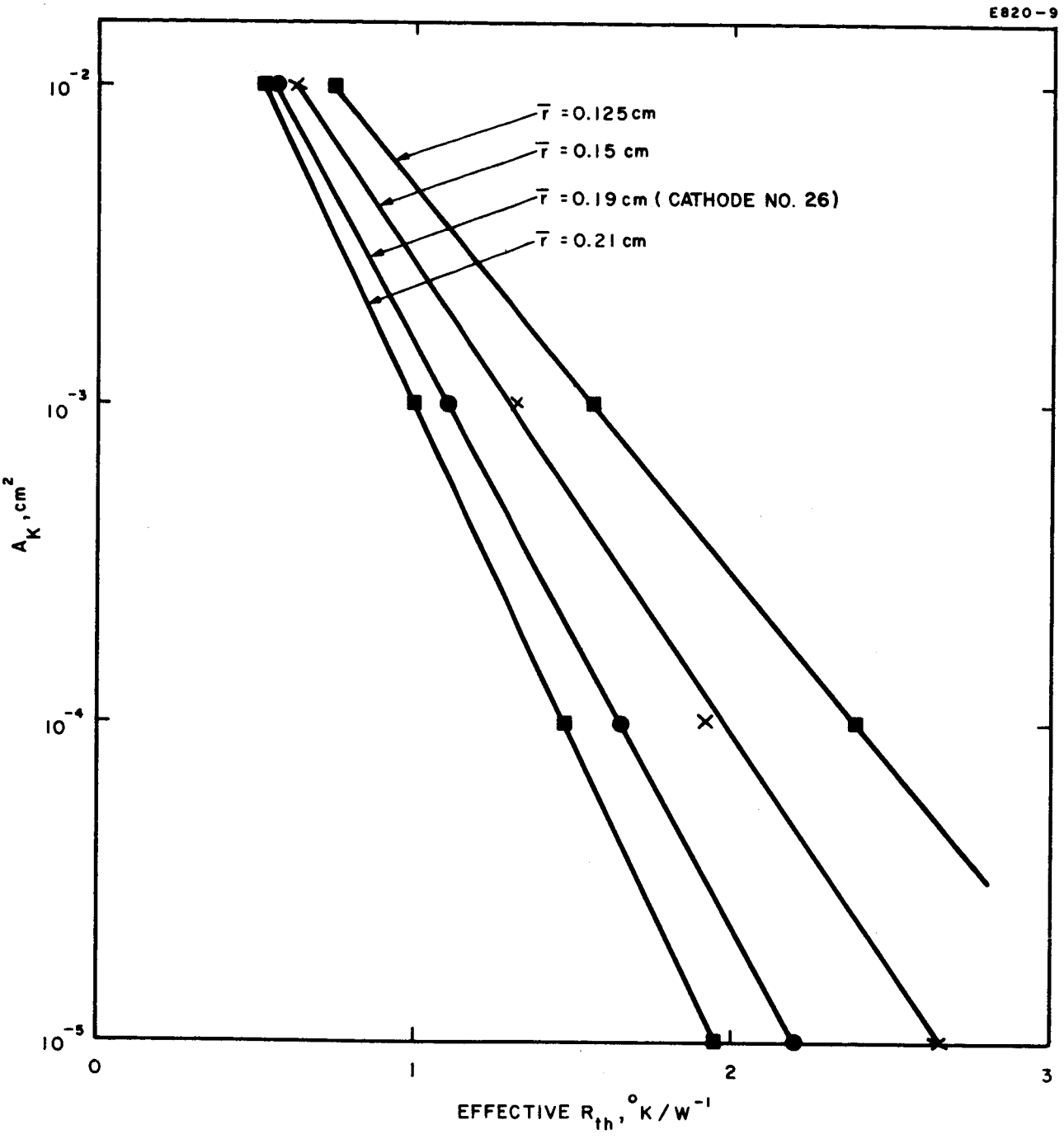

Fig. 10. Effective cathode thermal resistance as a function of mercury surface area.

D. - Variation with Beam Current

It is also pertinent to consider the variation of the temperature difference $T_{Hg}-T_K$ with the mercury pool temperature T_{Hg} for different values of I_B. In particular it is interesting to compare the relative merits of circular and annular cathode geometry for relatively small I_B.

From the relationship

$$A_K = I_B/eL_a \eta_m$$

A_K can be determined as a function of T_{Hg}. This is independent of the geometry of A_K and is shown in Fig. 11 for three values of I_B. It can also be seen from the figure that the function is relatively insensitive to a change in η_m from 100% to 80%, so that for clarity the curves for I_B = 400 mA and 200 mA are shown for η_m = 90% only. Again choosing Cathode No. 26 (mean annular radius 0.19 cm) as representative of the annular configuration, combination of Fig. 11 with Figures 5 and 10 then gives the data for Figures 12 and 13.

Fig. 12 shows the relationship between T_{Hg} and the temperature difference $T_{Hg}-T_K$ for unit cathode specific heat loading $V_{K,th}$: In Figures 12 and 13 it has been assumed that η_m = 90% and the electron to atom ratio at the cathode, K_e/K_a = 12. The I_K values equivalent to I_B = 600, 400 and 200 mA are then 8.0, 5.33, and 2.66A respectively. For a particular value of I_B the curves for circular and annular cathode geometry merge at low values of T_{Hg}, but for practical temperatures (T_{Hg} from 130° to 300°C), annular geometry produces much smaller values of $(T_{Hg}-T_K)/V_{K,th}$ than does a circular geometry.

This is more clearly shown in Fig. 13, where the temperature T_K at the thermocouple junction has been drawn as a function of the pool temperature T_{Hg} for different I_B, assuming a constant value for $V_{K,th}$ of 5.0 WA^{-1} throughout, and again K_e/K_a = 12 with η_m = 90%. The ideal case - that of zero cathode thermal resistance - is given by the asymptote, and the relative merit of a cathode geometry can be judged by how closely the curves for a given I_B approach the asymptote. Again the curves for annular and circular cathode geometry merge at low T_{Hg}, but only those curves for annular geometry have any similarity with the asymptote for $T_{Hg} > 150°C$, that is for useful values of T_{Hg}. In fact for this temperature regime the curves for the circular cathode

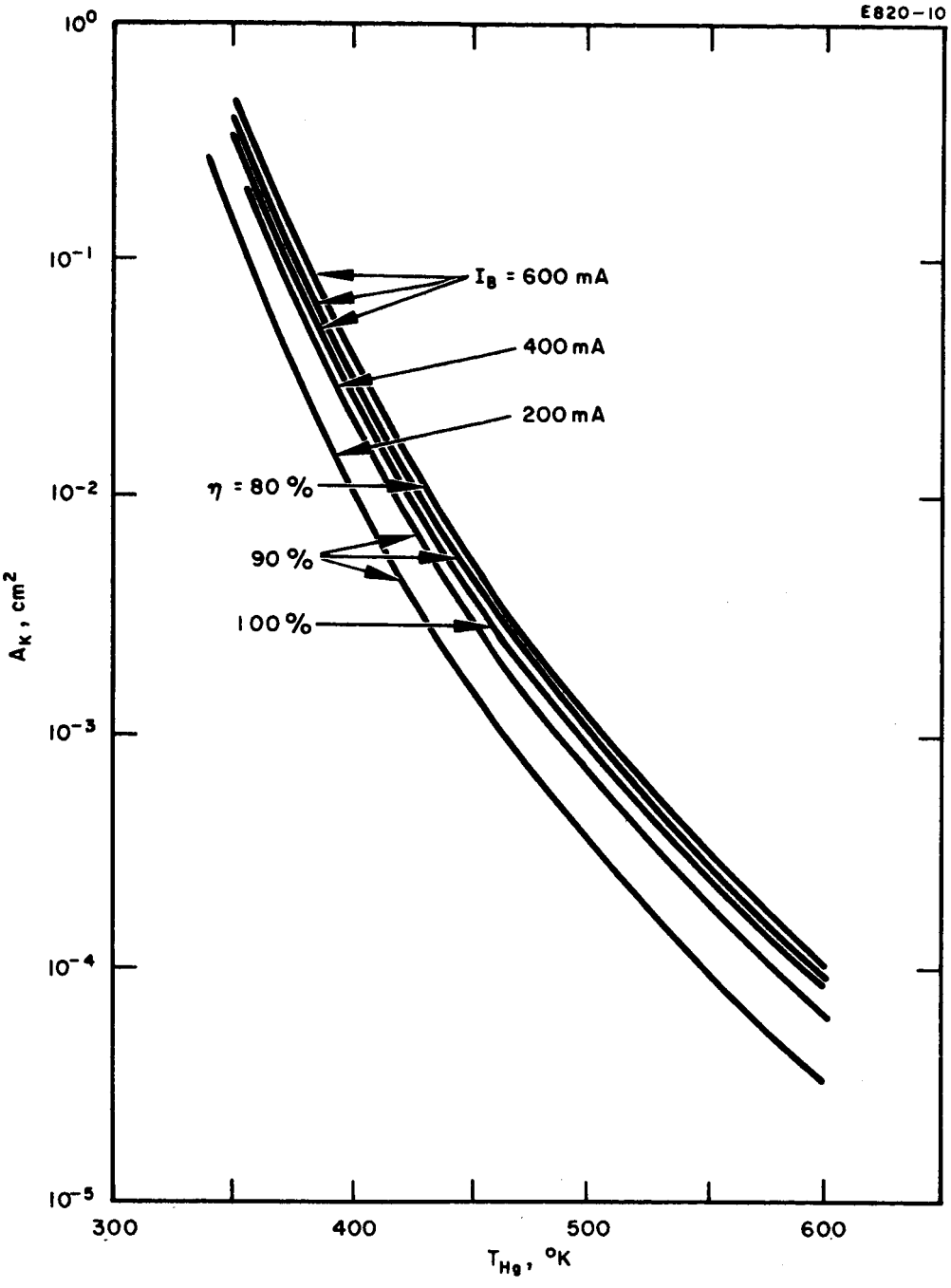

Fig. 11. Mercury surface area A_K as a function of T_{Hg} for different values of I_B and η_m.

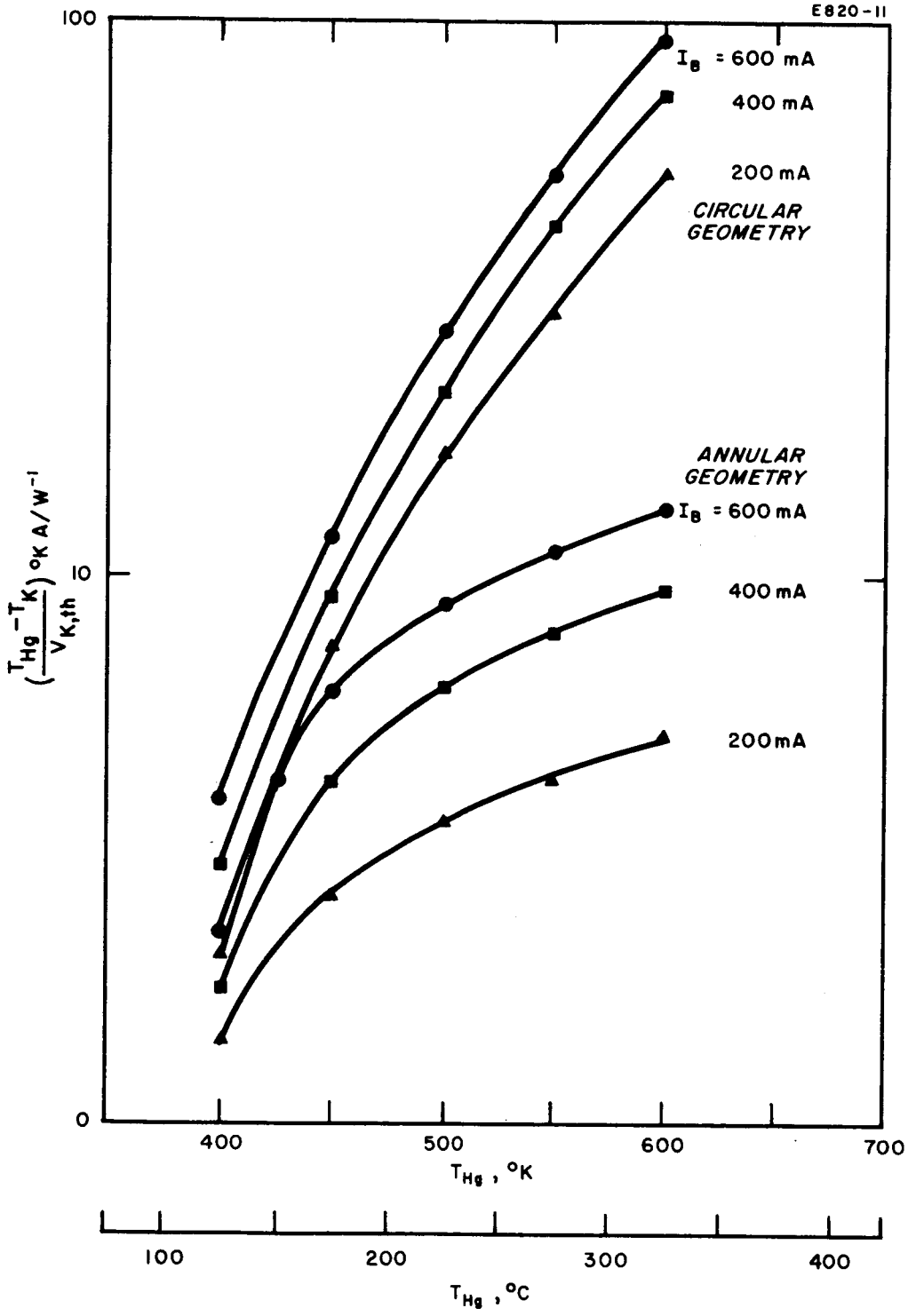

Fig. 12. Temperature difference $T_{Hg} - T_K$ per unit cathode specific heat loading $V_{K,th}$ as a function of T_{Hg}.

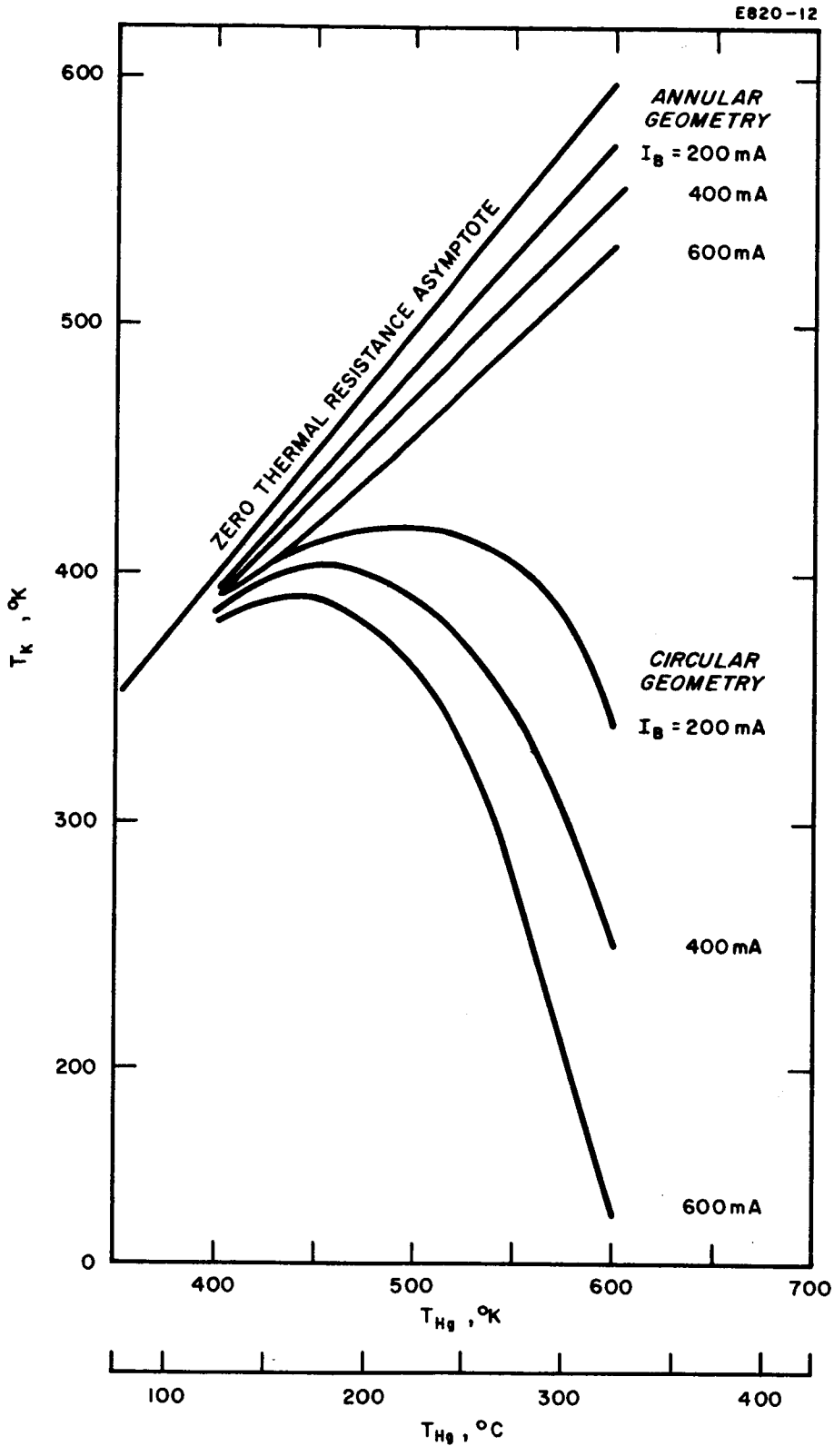

Fig. 13. T_K as a function of T_{Hg}.

depart strongly from the asymptote.

Later it will be shown that the main thermal resistance opposing the flow of $P_{K,th}$ occurs between the pool and the thermocouple junction: this means that T_K relates closely to the thruster shell temperature, which should be high to aid in heat rejection. Fig. 13 then shows the relative advantages of using annular rather than circular cathode geometry even for a thruster with a low I_B, and clearly demonstrates that heat rejection is always accomplished with a lower temperature difference when annular rather than circular geometry is used.

E. - The Outer Regions of the Cathode Matrix

The body of the cathode between the thermocouple junction and the radiating surface (thruster shell) is sketched in Fig. 14. To estimate the heat flow to the radiating edge C, it can be assumed that the isothermal surface through the thermocouple junction A is hemispherical, and that all other such surfaces are hemispherical as the radius y is increased to a distance equal to the thickness z_1 of the cathode matrix (point B). From B to C the isothermals can be thought of as being concentric cylinders.

Between A and B, the thermal resistance is

$$R_{th} = \frac{1}{2\pi k_{th}} \quad \frac{y_B - y_A}{y_A \; y_B} \quad ,$$

which becomes

$$R_{th} = \frac{z_1 - 0.44}{0.88 \, \pi \, k_{th} \, z_1}$$

taking point A to be about 0.44 cm from the center line. Fig. 15 shows the ΔT between points A and B as a function of the power input to the cathode for some practical values of z_1, assuming the material to be molybdenum.

From B to the outer edge the thruster end plate may well be aluminum, with k_{th} = 2.3 W/^{o}Kcm and a density of 2.7 g/cm^3. If the thickness of the cathode plate (z_2) remains constant (Fig. 14a) from B to C the thermal resistance is

$$R_{th} = \frac{1}{2\pi \, k_{th} \, z_2} \, \ell n \quad y_c / y_B \quad = \quad \frac{1}{2\pi \, k_{th} \, z_2} \quad .$$

For overall weight reduction, $z_2 < z_1$ seems likely. Alternatively, the thickness z_2 can be made a function of y (Fig. 14b), and if this is such that

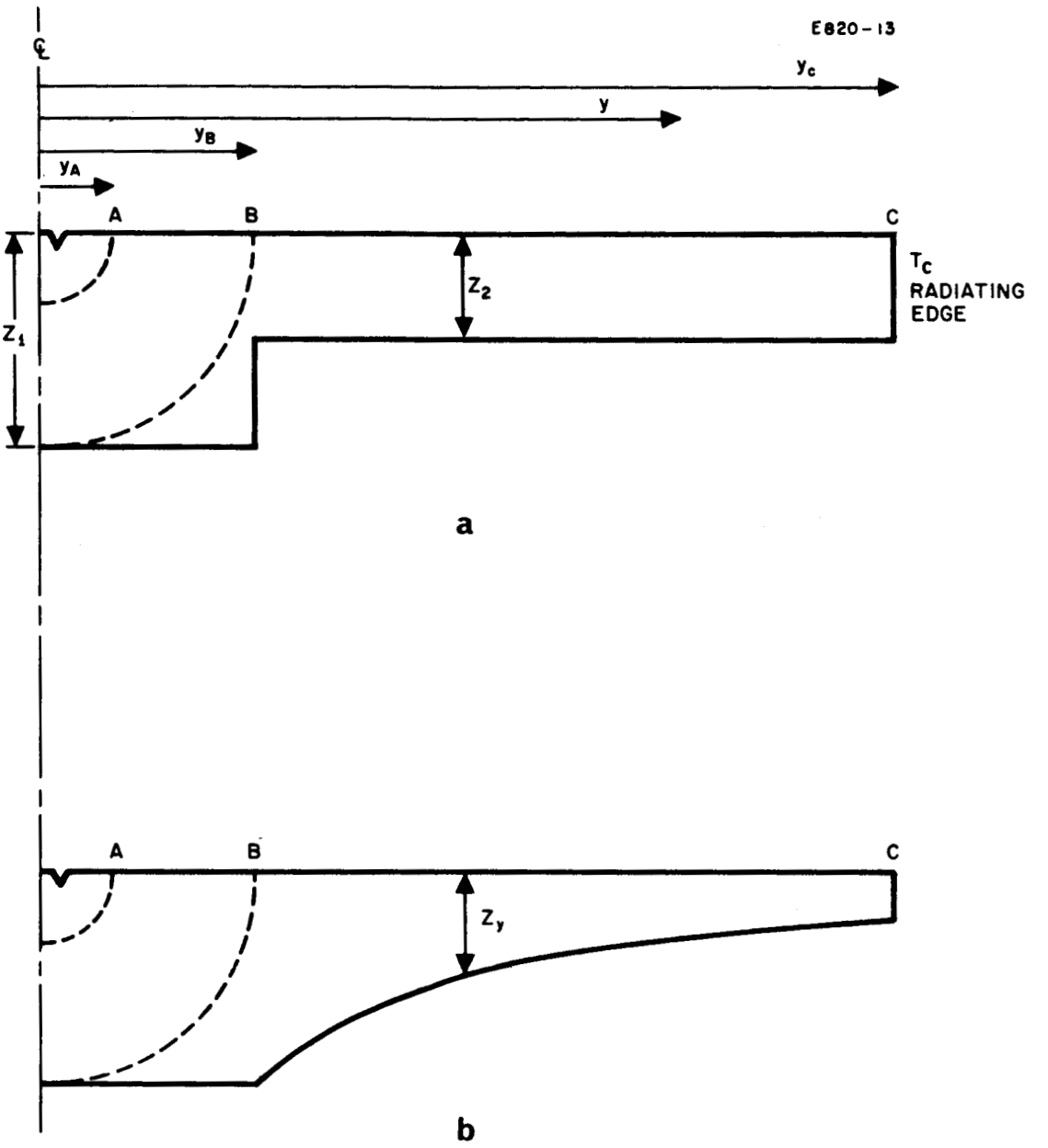

Fig. 14. Sketch of cathode outer regions.

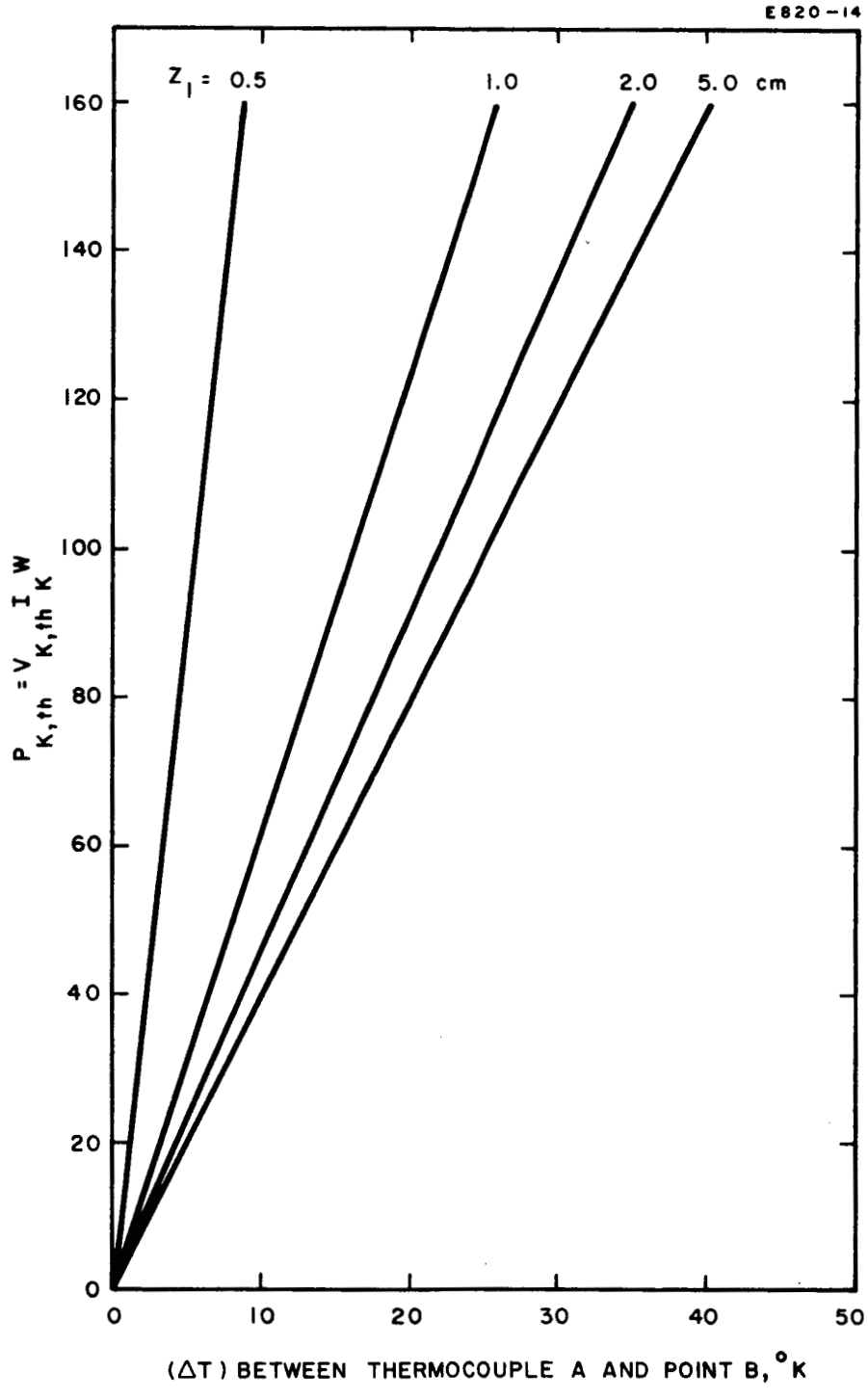

Fig. 15. Temperature difference ΔT between thermocouple point A and point B on cathode as a function of cathode heat flux $V_{K,th} I_K$.

$$yz = \text{constant},$$

the thermal resistance becomes merely

$$R_{th} = \frac{y_c - z_1}{2\pi k_{th} z_1^2} \quad .$$

Figs. 16 and 17 show the temperature difference between B and C as a function of the power input, for various geometries.

The overall temperature difference between the mercury pool and the radiating surface can also be plotted as a function of the weight of the cathode and end plate structure: Fig. 18 shows this for a number of geometries, and shows that a good compromise between weight and heat conduction can be effected when z_1 = 1 cm and z_2 lies between 0.2 and 0.5 cm.

F. - The Overall Thruster

In a 20 cm diameter thruster I_B is typically 600 mA; let us assume a mass utilization of 90% at 450 eV/ion. For an electron-to-atom ratio of 12, I_K = 8A, V_D = 33V, the total power input to the thruster = 264W. With a cathode operating at $T_{Hg} = 300^{\circ}C$, A_K is equal to 1.6×10^{-4} cm^2.

The temperature of the thruster shell can be expressed as a function of the weight of the cathode plus the shell assuming a value for the cathode heat input $V_{K,th} I_K$ and a fixed mercury temperature of $T_{Hg} = 300^{\circ}C$. This is shown in Fig. 19 for different values of $V_{K,th}$, and shows that the shell temperature can be as high as $175^{\circ}C$ for close to minimum weight even with $V_{K,th} = 7.5\ WA^{-1}$. For 90% effective shielding between the anode and the aluminum shell, the heat rejected by the shell (including that from the anode) must be about 60W when $V_{K,th} = 5\ WA^{-1}$ and 80W when $V_{K,th} = 7.5\ WA^{-1}$: this can be achieved easily for an oxidized aluminum shell radiating over 2π steradians into free space.

For increased thrust the possibilities exist of either increasing the engine diameter or of mounting engines of, for example, 20 cm diameter, in an array. In the case of a pheripheral array of 20 cm thrusters shown in Fig. 20, loss of heat from the thruster shell is equivalent to radiation from about 1/3 of the surface area into a 2π solid angle. Calculations show that the shell can reject the same thermal power as above at temperatures of $\leq 200^{\circ}C$ if the emissitivity of the thruster shell is increased to 0.9 by painting with one of several commercially available materials. At this shell temperature

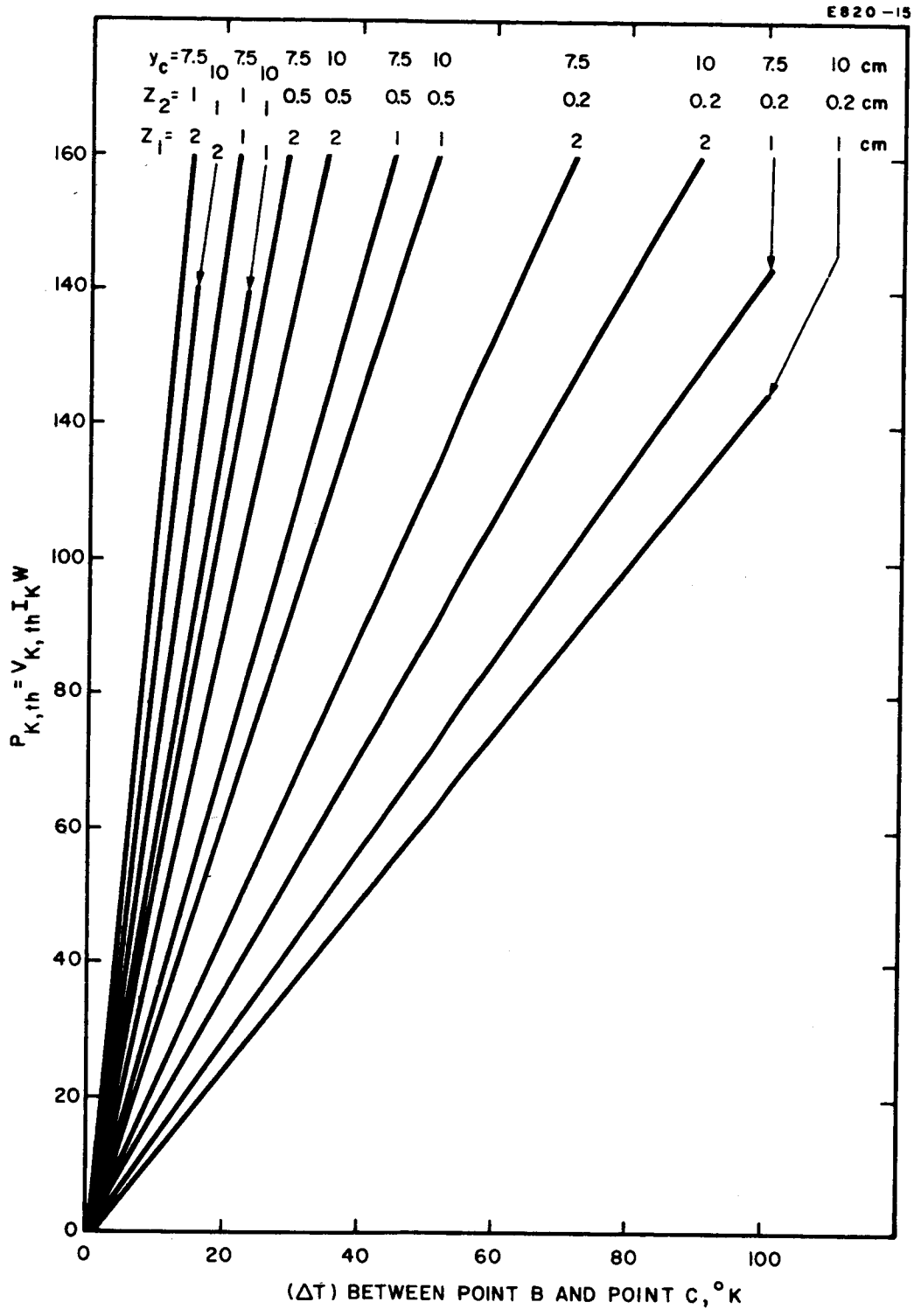

Fig. 16. Temperature difference ΔT between B and C as a function of cathode heat flux $V_{K,th} I_K$.

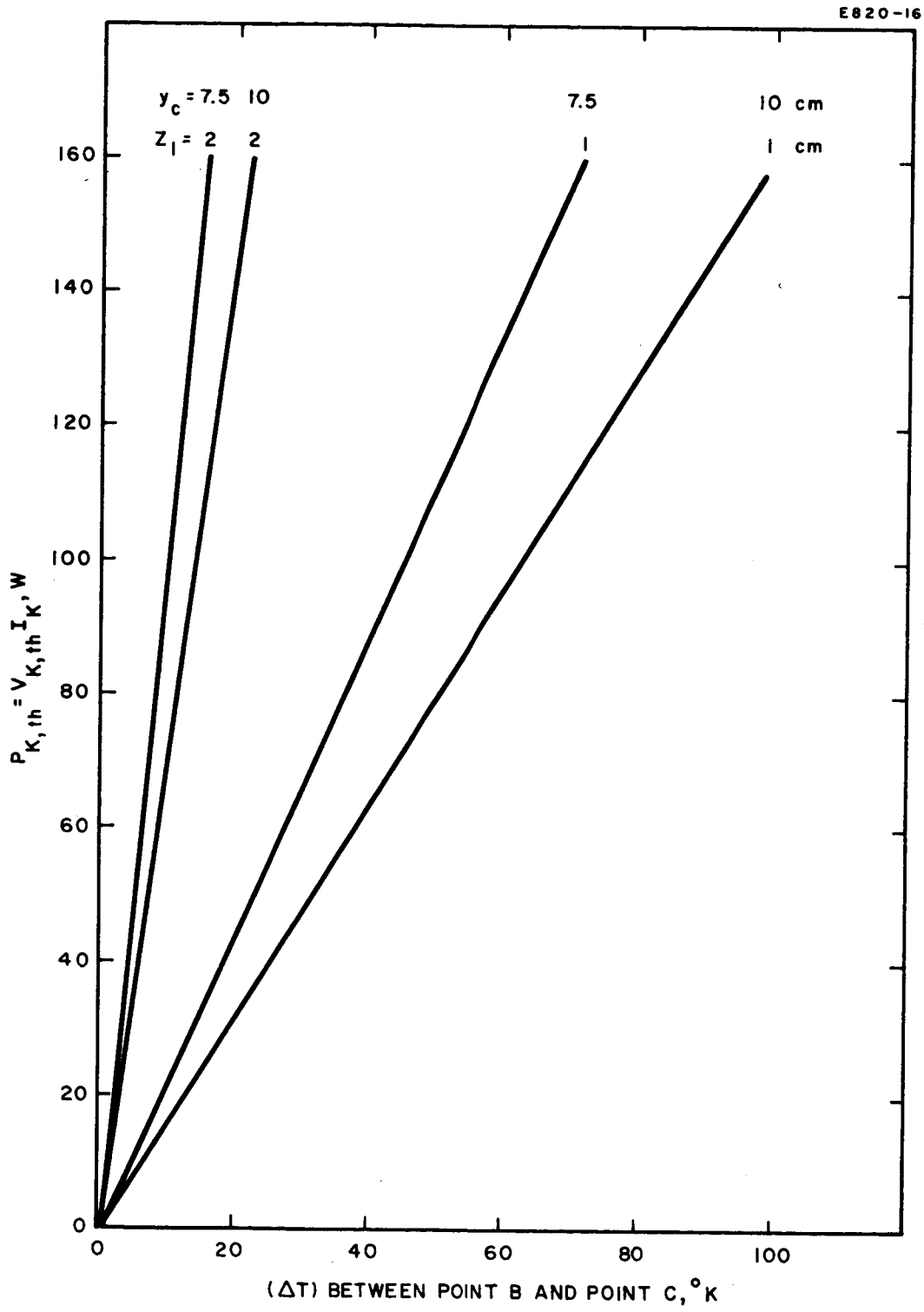

Fig. 17. Temperature difference ΔT between B and C as a function of cathode heat flux $V_{K,th} I_K$.

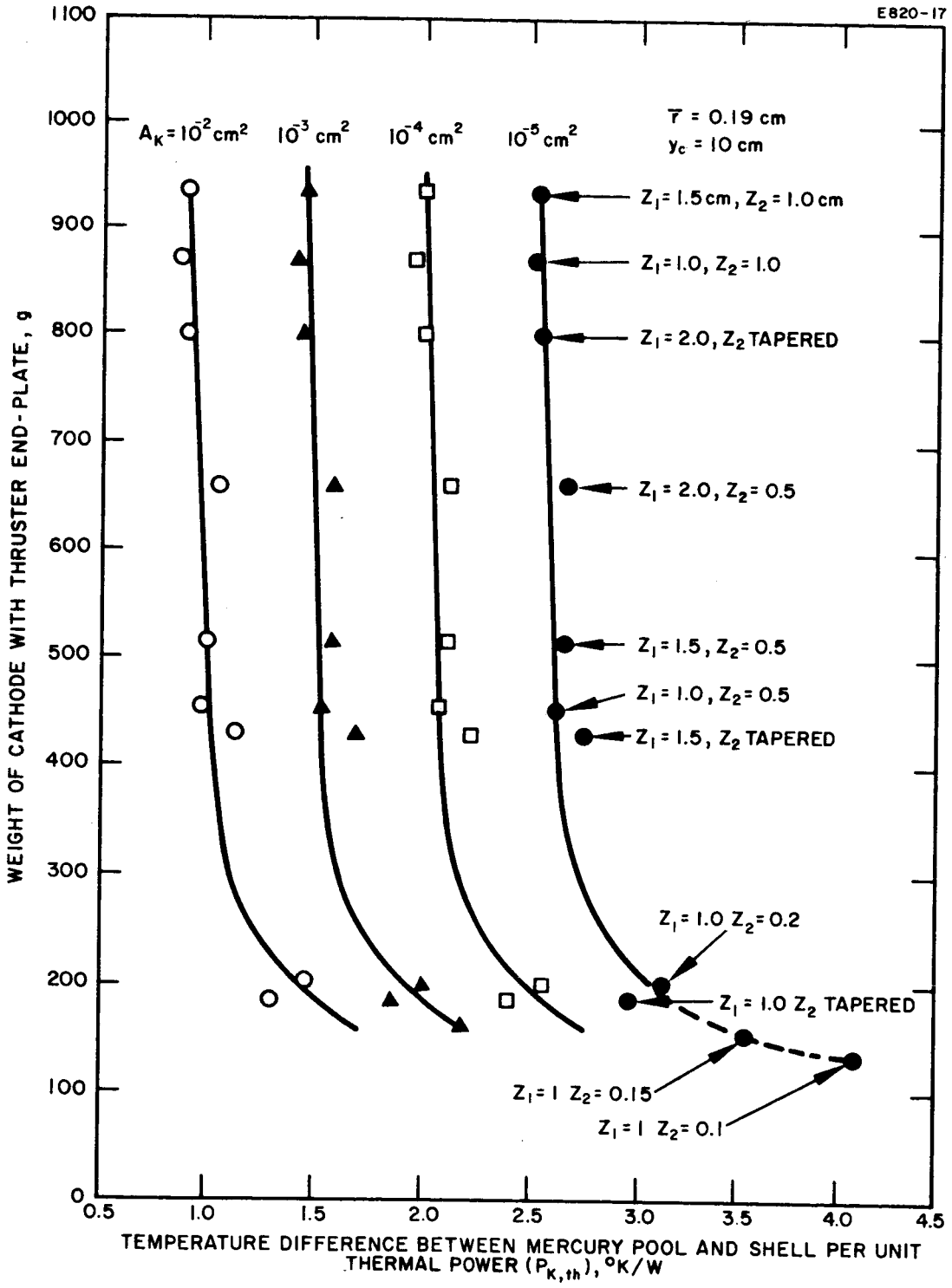

Fig. 18. Temperature difference ΔT between cathode and sink as a function of cathode weight.

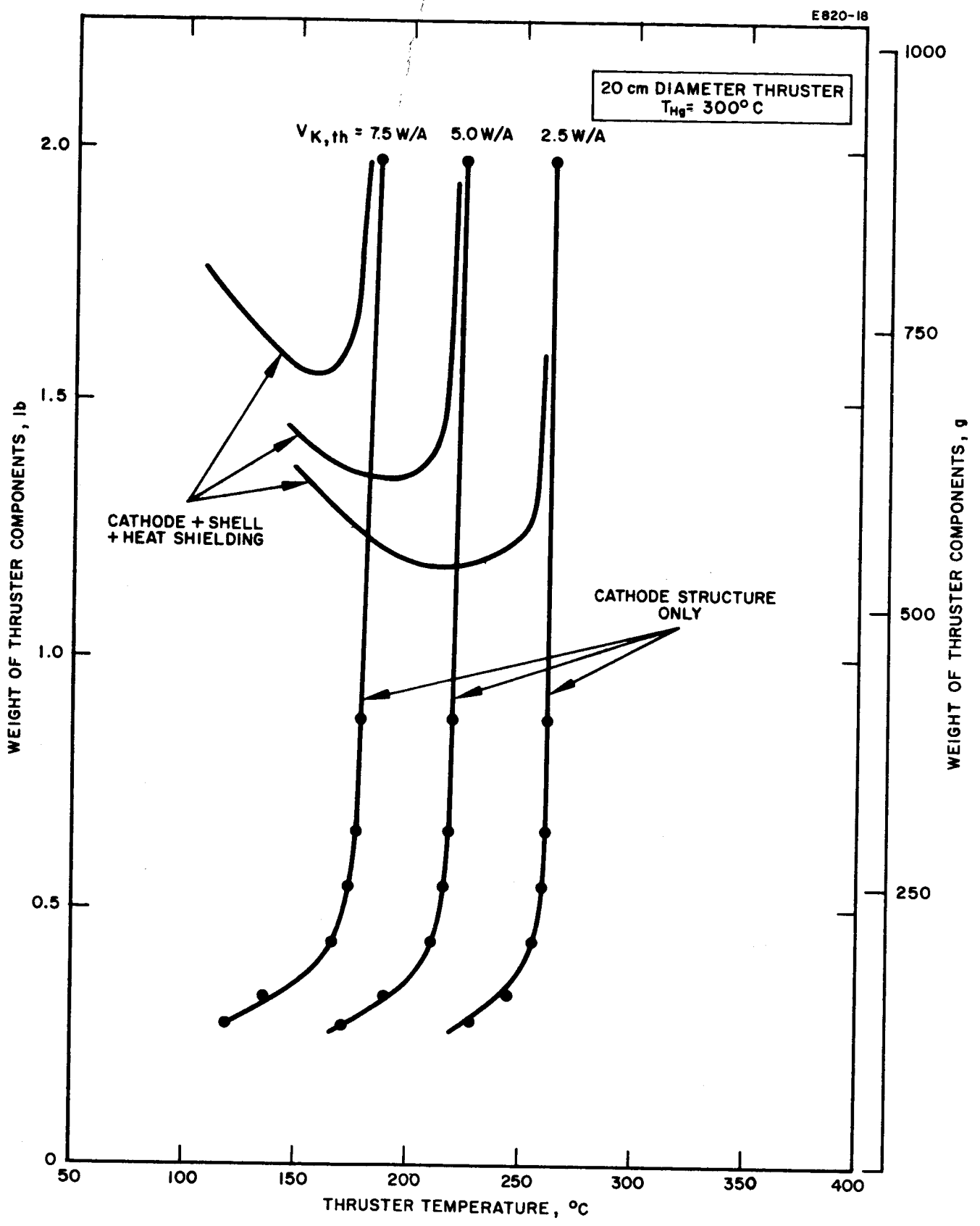

Fig. 19. Thruster shell temperature as a function of weight of thruster components.

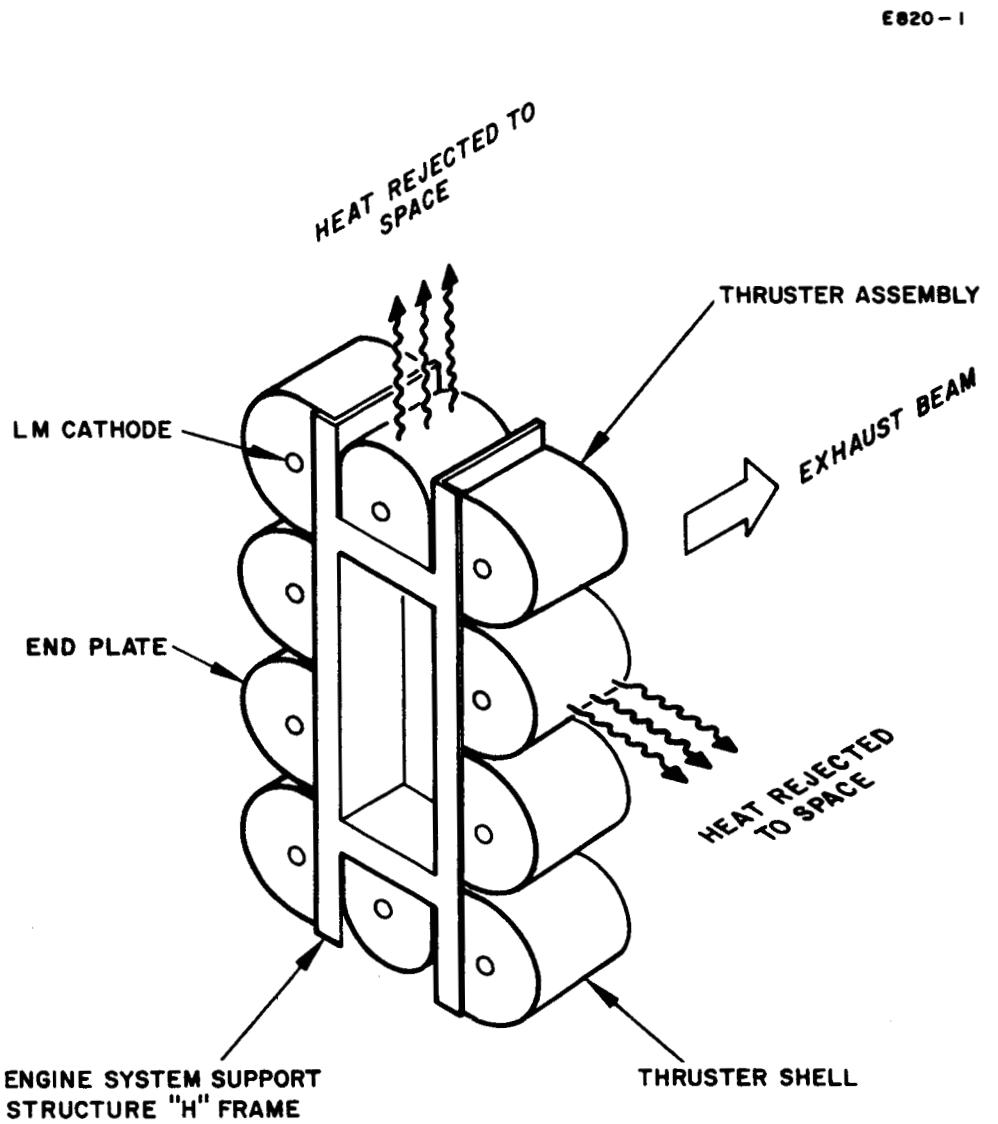

Fig. 20. Peripheral array of 20-cm diameter thrusters.

the additional rise due to solar exposure at 1 a.u. is 17°C, representing only a 3% perturbation of the absolute cathode temperature T_{Hg}.

G. -Conclusions

It can be seen from this analysis that an annular liquid mercury cathode operating at T_{Hg} = 300°C can reject heat to a sink at 200°C at an economical overall weight. In contrast the circular cathode experiences a severe temperature drop in the immediate cathode matrix and must be operated with a substantially lower sink temperature: thus it would not be suitable for incorporation into an array, where the radiating portion of the shell area is effectively less than in the freely radiating case.

For a given T_{Hg}, the temperature difference between the cathode and sink depends on the mercury surface area A_K and the annular diameter. These values are determined by the thruster parameters I_B, η_m and K_e/K_a. Applying the weight optimization procedure outlined above to a 20 cm LM thruster leads to an overall thruster weight of about 8 lb.* This thruster mounted in a peripheral array would be capable of rejecting the estimated cathode and anode heat flux, even under maximum solar exposure.

---

* This applies to a thruster with 600 mA beam current and K_e/K_a = 12. At a specific impulse of 4000 sec, η_m = 90% and a thruster power efficiency of 82% (450 eV/ion), the corresponding weight to power ratio would be 5.3 lb./kW.

III. HIGH-TEMPERATURE LM CATHODE RESEARCH AND DEVELOPMENT

A. -Main Thruster Cathode

1. -Derivation of a normalized performance parameter

In order to make meaningful comparisons of cathode performance between different cathodes or before and after modifications of cathode geometry, allowance must be made for different operating conditions. This can be done by specifying a fixed set of normalized operating conditions, choosing one suitable performance parameter, and transforming its measured value to a normalized value. We have selected the temperature of the radiating thruster shell, the thermal resistance of the thruster end plate, and the current drawn from the cathode as the fixed conditions, because these parameters are dictated by thermal and weight considerations regarding the spacecraft and by thruster (rather than cathode) design. We have chosen the electron-to-atom emission ratio as the performance factor to be normalized (while retaining the measured value of the specific thermal loading of the cathode), because on the one hand this ratio is affected by changes in all other parameters, thus representing a compound measure of cathode performance, and on the other hand its normalization is amenable to analytical formulation without undue approximations.

We use the following notation:

K_e/K_a = electron-to-atom emission ratio

I_K = current drawn from cathode

$P_{K,th}$ = thermal power delivered to cathode

$V_{K,th} = P_{K,th}/I_K$ = equivalent voltage, expressing specific thermal loading of cathode

p_{Hg} = vapor pressure over exposed Hg surface in cathode

T_{Hg} = temperature of exposed Hg surface in cathode

T_K = temperature of cathode at thermocouple location

T_T = temperature of radiating thruster shell

$\Delta_K T = T_{Hg} - T_K$ = temperature difference within cathode

$\Delta_T T = T_K - T_T$ = temperature difference within thruster end plate

$R_{th,K} = \Delta_K T/P_{K,th}$ = thermal resistance of cathode

$R_{th,T} = \Delta_T T/P_{K,th}$ = thermal resistance of thruster end plate

e = elementary charge

Subscripts:

m = measured

n = normalized

First, we note that

$$K_e = I_K/e \qquad \text{and } K_a \propto p_{Hg}\,(T_{Hg}),$$

where the latter is true for a fixed position of the exposed mercury surface in the pool-keeping structure. Next, we observe that we have the following functional dependences:

$$T_{Hg} = T_{Hg}\,(T_K,\ I_K, V_{K,th},\ R_{th,K}),$$

and

$$T_{Hg} = T_{Hg}\,(T_T, I_K,\ V_{K,th},\ R_{th,K},\ R_{th,T}).$$

Therefore, we can write for the measured and normalized electron-to-atom emission ratios, respectively:

$$\left(\frac{K_e}{K_a}\right)_m \propto \frac{I_{K,m}}{p_{Hg}\left[T_{Hg}\,(T_{K,m},\ I_{K,m},\ V_{K,th,m},\ R_{th,K})\right]},$$

$$\left(\frac{K_e}{K_a}\right)_n \propto \frac{I_{K,n}}{p_{Hg}\left[T_{Hg}(T_{T,n},\ I_{K,n},\ V_{K,th,m},\ R_{th,K},\ R_{th,T})\right]}.$$

In writing these expressions, we make the assumption that a fixed position of the exposed mercury surface results in a fixed value of the specific thermal loading. At least for the current range to which the normalizing procedure will be applied, this appears to be a reasonable approximation. We then have the following self-explanatory equations:

$$\left(\frac{K_e}{K_a}\right)_n = \left(\frac{K_e}{K_a}\right)_m \cdot \frac{I_{K,n}}{I_{K,m}} \cdot \frac{p_{Hg}\left[T_{Hg}(T_{K,m}, I_{K,m}, V_{K,th,m}, R_{th,K})\right]}{p_{Hg}\left[T_{Hg}(T_{T,n}, I_{K,n}, V_{K,th,m}, R_{th,K}, R_{th,T})\right]},$$

$$T_{Hg} = T_T + \Delta_T T + \Delta_K T = T_K + \Delta_K T,$$

$$\Delta_T T = I_K V_{K,th} R_{th,T} \quad , \quad \Delta_K T = I_K V_{K,th} R_{th,K} .$$

With these, plus a table or graph for the saturated vapor pressure of mercury as a function of temperature, we can now present our experimental results in a normalized form, and we have done this in Section IIIA-5 below.

From the standpoint of purely thermal requirements in the thruster applications, a cathode performs the better the higher its $(K_e/K_a)_n$; from the standpoint of both thermal and efficiency requirements, cathode performance must be judged in terms of both a high $(K_e/K_a)_n$ and a low $V_{K,th}$.

2. -Modifications in cathode geometry

During the reporting period, Annular Cathode No. 26 was modified in two respects. One revision was to shorten the narrow mercury passage leading to the divergent nozzle section. This resulted, as expected, in operation similar to that experienced with Cathode No. 25 after the corresponding modification, i.e., full circle arc operation could instantly be attained. The second revision was to remove the surface comprising the inner wall of the annular divergent nozzle. (This second revision was a step beyond No. 25 modifications so far.) Both modifications have led to a substantial performance improvement, as demonstrated by the measurements presented in the test results section farther on. It was noticed that Cathode No. 26 ran satisfactorily at a somewhat higher current after modification than before, which was due to a slight enlargement of the annular gap during repolishing.

3. -Electrical pulse igniter

Contributing to the successful evaluation of LM cathodes at high temperature was the introduction of high voltage pulses for arc initiation. With the new ignition circuit, cessation of the arc current energizes a relay which in turn completes a circuit furnishing rapid, high voltage pulses to a stationary igniter electrode placed in front of the cathode. The arc usually needs only one pulse to restart under normal operation, and placement of the

igniter electrode relative to the cathode does not demand more than reasonable initial adjustment.

The electrical pulse ignition system is fully applicable to thruster operation. A flight-type system will use a vacuum potted pulse transformer (also demonstrated) and silicon controlled rectifiers instead of electro-mechanical relays.

4. - Vapor feeding of high-temperature LM cathodes

Experiments performed some time ago under Company-sponsored programs have shown that circular LM cathodes operating at high currents ($\approx$ 150 A) and high degrees of spot-pattern contraction (corresponding to current densities $\gtrsim 10^4$ A cm^{-2} averaged over the exposed mercury area) can switch under certain thermal conditions spontaneously into a different mode, which will be referred to here as the "diffuse spot-pattern" or "DSP" mode in order to distinguish it from the normal "linear spot pattern" or "LSP" mode. In these experiments a high current discharge was started with the mercury surface being large compared with the feed channel area. As the mercury contained in the pool-keeping structure was used up, the cathode spot pattern shrank to the size of the channel, and then the arc spot pattern became diffused, i.e., the cathode glow was distributed quite uniformly over an area, rather than concentrated along a line. In this mode the mercury surface is below the mouth of the channel, but copious evaporation keeps the discharge supplied with vapor.

We believe that in this mode the random motion of the individual arc spots is distributed over the entire luminous area, rather than restricted to a line, so that the time-averaged current density in the diffuse spot pattern is reduced by orders of magnitude from the level associated with the linear spot pattern.

The spots are believed to exist by virtue of a transient condensation of mercury vapor on the walls of the pool-keeping structure. It may not be necessary for a heavy condensation of mercury vapor to occur because electron emission (if it is caused, for example, by excited mercury atoms impinging on the cathode) could occur without a complete, macroscopic covering of mercury over molybdenum: the work function of molybdenum (4.4 eV) is less than the metastable potential of mercury (4.67 eV) so that electron emission is ener-

getically possible at a reasonable yield.*

On the basis of these considerations, we concluded that it should be possible to separate spatially the region where vapor is evolved from a free mercury surface and the region where transient recondensation of this vapor permits electron emission in the diffuse spot-pattern mode - in other words, it should be possible to vapor-feed (rather than liquid-feed) an LM cathode operating in the DSP mode.

This possiblity is of special interest because it promises several advantages over liquid-fed LSP-mode LM cathodes in thruster operation:

(a) Higher thruster efficiency and lower specific thermal loading should result from thermally decoupling the pool-keeping structure from the evaporator, because the required electron-to-atom emission ratio may be obtained with less vapor flow constriction (and hence, less plasma losses) downstream from the electron-emitting zone.

(b) A vapor-fed LM cathode could use the same feed system and isolator as is used for electron-bombardment thrusters with other cathode types, thus permitting more flexibility in cathode choice for these thrusters up to late stages of design freezing.

(c) It may be possible to achieve such high electron-to-atom emission ratios that only a fraction of the total expellant flow needs to be fed through

---

* Optically similar phenomena, observed on spot anchors with conventional pool cathodes at much lower currents and in the presence of strong axial magnetic fields, were described by C. G. Smith[+] and K. G. Hernqvist[‡]; the latter author termed this type of discharge the "dispersed" or "D" mode and established an upper current density limit of $\approx 10^2$ A cm^{-2} for this mode. Our much higher current densities, as well as other observations reported below, lead to the conclusion that the dispersed mode and the diffuse spot-pattern mode are not identical. One might say that in the D mode the spot itself is dispersed over a relatively large area, resulting in a considerable change in the emission mechanism, while in the DSP mode only the pattern of the random spot motion is diffuse, leaving the conditions during the life of an individual spot substantially unchanged.

+ Smith, C. G., Brit. J. Appl. Phys. 4, 252 (1953).

‡ Hernqvist, K. G., Phys. Rev. 109, 636 (1958).

the cathode. (This is a consequence of the reduced thermal power input density in the DSP mode, compared with the LSP mode.) The resulting design freedom for the expellant injection pattern should result in additional thruster efficiency improvements, as well as in complete interchangeability between LM and other cathodes, without any thruster modifications.

The listed advantages have prompted us to substitute a vapor feed system for the liquid feed system used with Cathode No. 26 in order to obtain some first-order experimental results. The feed system conversion was accomplished by omitting the flow impedance, electron-beam welding a stainless-steel vaporizer mesh into the feed line, and wrapping a heater around the feed line portion between vaporizer and cathode. The same mercury reservoir was used as with the liquid feed system, thus permitting accurate flow rate measurements within time intervals of a few minutes. The feed system was kept under a constant pressure ($\approx$ 1 psig), and the flow rate was adjusted by varying the vaporizer temperature. Even though no modifications on the cathode proper were made, the results of our experiments are extremely encouraging; they are listed in the following section. The electrical pulse ignitor proved to be usable also for the vapor-fed LM cathode without modification. One important observation is that the discharge starved out when the temperature was raised too high for a given flow rate, indicating the importance of transient condensation as postulated above for the DSP mode, and in contrast to the expectations for Hernqvist's D mode.

5.-Test results in diode operation

A comprehensive presentation is given in Table I of all those high-temperature LM cathode diode measurements which included determinations of the specific thermal loading. Roman numerals are used to indicate changes in diode geometry, with the following meaning: I indicates the original shape as shown schematically in Fig. 2. II designates the modification of the uniformly narrow mercury flow passage shown in this Fig. to a narrow passage of minimum depth, fed by a wider passage. III indicates stage-II modification plus truncation of the inner cone of the pool-keeping structure at the downstream end of the narrow flow passage.

The table lists the directly measured parameters and the normalized electron-to-atom emission ratio as defined in Section IIIA-1. For the smaller one of the two cathodes the normalization has been carried out for two cases: (a) Operation in a 15-cm diameter thruster at $I_{K,n} = 6A$, with $T_{T,n} = 225^{o}C$ and $R_{th,T} = 0.7^{o}K\ W^{-1}$. (b) Operation in a 20-cm diameter thruster at $I_{K,n} = 8A$, with $T_{T,n} = 250^{o}C$ and $R_{th,T} = 1.0^{o}K\ W^{-1}$. Both cases correspond to thrusters operating in relatively dense clusters, see Sec. II, and case (a) represents a relatively unfavorable discharge-to-beam current requirement. For both cases and both cathodes, $R_{th,K} = 1.66^{o}K\ W^{-1}$ was assumed (see Sec. II).

Inspection of Table I leads to the following conclusions:

(1) Cathode No. 25-II can meet and exceed all temperature and K_e/K_a requirements of 15-cm thrusters, even under unfavorable conditions.

(2) With this cathode, further minimization of $V_{K,th}$ (and the associated discharge voltage differential) can be expected to result in thruster efficiency improvements on the order of 100 eV/ion for case (a).

(3) The same cathode cannot meet equally rigorous requirements for operation in a 20-cm thruster.

(4) Cathode No. 26 can meet and, in its stage III, considerably exceed all thermal and emission ratio requirements of 20-cm thrusters, including the most unfavorable conditions. It should perform satisfactorily also in considerably larger thrusters.

(5) In liquid-fed operation of this cathode, minimization of $V_{K,th}$ can be expected to result in thruster efficiency improvements on the order of 50 eV/ion for case (b). This conclusion is in excellent agreement with the experimental comparison of Cathode No. 26 with the water-cooled life-test cathode (see Quarterly Report No. 2).

(6) Approximately one-half of this possible improvement may already be realizable by vapor-feeding of the same cathode, as evidenced by tests No. 13 & 15. (No thruster tests have been performed yet.). A similar prediction can also be made for vapor-feeding of Cathode No. 25.

(7) The monotonic increase of the normalized performance parameter as a function of cathode geometry evolution fully justifies the steps taken during this evolution.

Test No.	Cathode Type	Feed Method	$T_{K,m}$ °C	$I_{K,m}$ A	$V_{K,th,m}$ WA^{-1}	$\left(\frac{K_e}{K_a}\right)_m$	$\left(\frac{K_e}{K_a}\right)_{n\ 15cm}$	$\left(\frac{K_e}{K_a}\right)_{n\ 20cm}$
1	25-II	Liquid	250	5.0	4.7	10	11	4.7
2	"	"	300	5.3	11	12	18	5.7
3	"	"	"	8.6	12	10	25	6
4	"	"	"	9.0	10	10	28	7.6
5	26-I	"	"	12.8	7.6	13		17
6	"	"	"	9.8	6.1	16		18
7	"	"	"	9.2*	10.6	17		12
8	26-III	"	"	15.8	8.3	21		34
9	"	"	"	10.5	7.1	41		45
10	"	"	"	21	9.7	31		83
11	"	"	"	23	9.7	28		91
12	"	"	375	16.3	8.7	20		70
13	"	Vapor	300	14.0	5.3	10	n.a.+	n.a.+
14	"	"	"	11.3	4.6	10	"	"

* Spot pattern only half circle.

+ The normalization principle (Sec. IIIA-1) is limited to the liquid-fed case.

TABLE I: Diode test results. All tests have lasted for several hours (typically 4 to 7).

(8) The table clearly shows the trade-offs between the various parameters. For example, test No. 7, compared with No. 6, shows the detrimental effect on $(K_e/K_a)_n$ and $V_{K,th,m}$ caused by partial utilization of the available spot-pattern length; and test No. 12 shows both the feasibility of operation at even-higher temperatures and the associated penalty.

B. -LM Cathode Neutralizer

The operating temperature of an LM cathode neutralizer in space is expected to be in the vicinity of 100°C, assuming that it can radiate waste heat only from its exposed face. It is one objective of this effort to demonstrate that LM cathode neutralizers can operate at such temperatures with high electron-to-atom emission ratios.

We have previously operated an LM cathode neutralizer at room temperature for over 500 hours as part of a thruster life test.* This neutralizer (shown in partial cross section in Fig. 21) was equipped with a mechanical automatic igniter, consisting of a solenoid-actuated tungsten tip which dipped into the exposed liquid mercury when the arc current was interrupted; it was subsequently pulled out in order to restrike the discharge.

While this type of igniter performed to full satisfaction on the main thruster cathode during the life test, its use on the neutralizer left much to be desired. Because of the approximately equal diameters of igniter and neutralizer pool-keeping structure, this mechanical action caused splashing of a considerable fraction of the small amount of liquid mercury contained in the pool-keeping structure when operating at the high K_e/K_a and low current wanted for neutralizer service. This, in turn, had two detrimental effects: (a) It permitted the arc to run on the splashed mercury globules outside the pool-keeping structure, resulting in frequent arc extinctions (followed by more splashing by the igniter and thus perpetuating the situation). (b) It limited the obtainable effective electron-to-atom emission ratio to a level far below the design value (even though the latter had been confirmed in experiments using careful manual ignition.

To confirm the contention that the predominant mercury loss mechanism was igniter splashing rather than evaporation, the neutralizer cathode was operated with the mechanical igniter at temperatures ranging from 20°C up to 90°C. While the vapor pressure of mercury changes by two orders of magnitude over this temperature range, the temperature increase to 90°C resulted in a reduction of the obtainable effective electron-to-atom emission ratio by only a small factor ($\lesssim 2$), as expected. At currents of 600 to 700 mA (corresponding to typical 20-cm diameter thruster currents) a K_e/K_a up to 16 was maintained

---

* Under Contract NAS 3-6262.

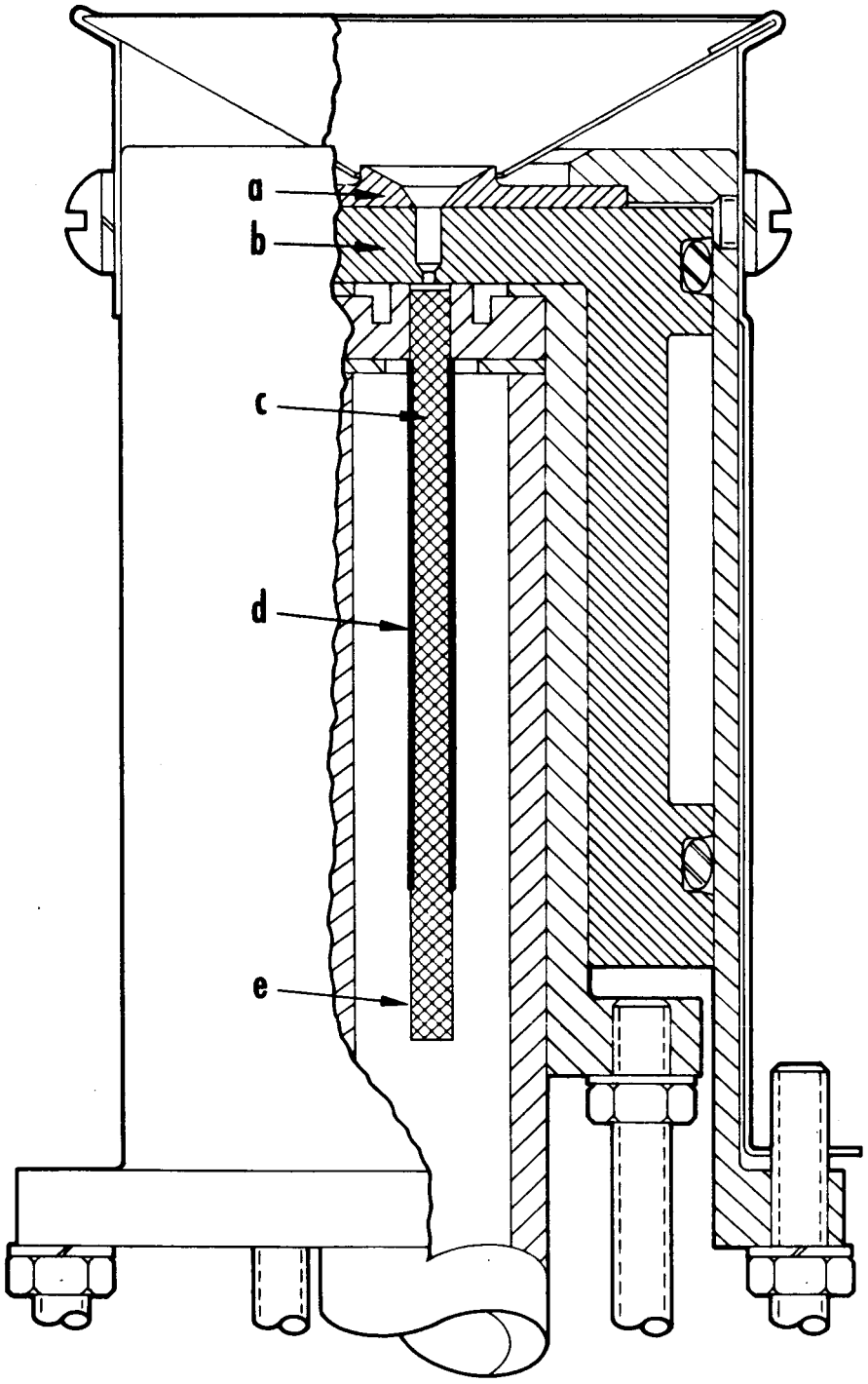

Fig. 21. Schematic cross-section of LM cathode neutralizer, not to scale. (a = refractory metal, b = permanently wettable metal, c = porous tungsten, d = sealed surface, e = open surface).

in runs of several hours duration at 90°C. This experiment, on the one hand, proved the importance of the mercury losses by splashing. On the other hand, it indicated (by the measurement of K_e/K_a up to 16 in the presence of splashing) the feasibility of efficient LM cathode neutralizer operation at the temperatures required for use in space, provided a non-mechanical igniter is used.

The electrical pulse igniter circuit described in Sec. IIIA was readily adapted to operation with a neutralizer cathode, the only major difference being in the sensitivity and current carrying capability of the discharge current sensor. The use of a pulse igniter immediately resulted in stable neutralizer operation without the frequent arc extinctions experienced before - and at the same time, it temporarily created a new problem:

In all neutralizer runs up to this time, a constant mercury flow was maintained by the same method as with the main thruster cathode, i.e., a constant pressure was applied to the storage reservoir, and a porous-tungsten flow impedance upstream of the pool-keeping structure permitted a mercury flow to pass which was (within the flow range of interest) a smooth function of the applied pressure. In order to shift the flow range where this smooth flow-pressure dependence exists to the level required for a neutralizer (one to two orders of magnitude below that of the main thruster cathode), it was necessary to use a flow impedance of $\approx$ 40 times higher value than that of the main thruster cathode. This higher impedance level was achieved with porous tungsten of the standard porosity by increasing the thickness of the flow-impeding layer by a factor of 20, and by reducing its cross-sectional area by a factor of 4. Continuous mercury flow with good uniformity was obtained when this type of flow impedance was used on a neutralizer with mechanical automatic igniter. When the electrical pulse igniter was used, however, it became impossible to obtain a steady flow rate in the proper range simply by adjusting the reservoir pressure (the flow was either zero or too high). Subsequent tests showed that the different behavior resulted from elimination of the frequent bursts of vibration which were caused by the mechanical igniter actuation.

A very appealing solution to this neutralizer feed problem was found during the flow-adjustment experiments. It was observed that when the feed pressure was first raised above the flow threshold and then lowered below the flow threshold of the porous-tungsten flow impedance (while monitoring the presence or absence of flow into the impedance with the position indicator of

the reservoir piston), mercury continued to be supplied to the neutralizer cathode at a uniform rate for several hours after the flow into the impedance had stopped. This was explained as the action of a small "capillary feed system", with the void volume of the porous-tungsten flow impedance serving as the mercury reservoir (see Fig. 21) and the permanently-wettable portion of the bi-metal pool-keeping structure serving as the wick. The rate of mercury flow into the pool-keeping structure was found to be adjustable by varying the temperature of the heat-exchanger jacket (which controls the temperature of both the pool-keeping structure and the porous tungsten rod). The required temperatures were between 65 and 80°C. Thus, feed rates compatible with discharge currents ranging from 250 mA to several amperes have been produced, and stable operation without discharge extinction has been demonstrated for many hours.

In order to measure the approximate electron-to-atom emission ratio for neutralizer cathode operation in the capillary-feed mode, we have operated the cathode continuously from the time when the capillary reservoir was refilled until the time when the cathode starved out. Assuming on the one hand that starvation meant absolute depletion of all voids in the porous tunsten rod and in the pool-keeping structure, and on the other hand that the absence of piston movement meant that no mercury was entering the porous tungsten rod, we have computed K_e/K_a from the known void volume and the operating time to starvation. The following typical results were obtained:

Neutralizer current:	0.6A	0.6 & 1.5A (0.9A aver.)	1.45A	1.5A	2.5A
Discharge voltage:	20V	20.5V	21V	21.5V	18.5V
Run duration:	4.0h	4.75h	1.85h	3.33h	1.58h
K_e/K_a:	53	94	59	110	87
No. of spontaneous extinctions during run (automatically reignited):	2	0	0	0	0

We have also attempted to measure the mercury volume required for refilling the capillary reservoir, but with the present arrangement it was found impossible to refill without overshooting by a relatively very significant amount. (The total capillary reservoir volume is only ≈ 0.025 cm^3, and the overfed volume may easily be 3 to 4 times larger.) Without any correction for this over-

shooting, the absolute lower limit for K_e/K_a during the run listed in the second column above is 24, and even this figure is quite competitive.

In conclusion it can be stated that stable LM cathode operation in the neutralizer current range has been demonstrated, with very attractive electron-to-atom emission ratios and power expenditures, at temperatures close to the equilibrium temperature of a neutralizer which is cooled only by radiation from its face. Therefore, the development of a mission-sized capillary feed system for this neutralizer appears to be warranted.

IV. THRUSTER TESTING OF HIGH TEMPERATURE LM CATHODES

A. -15-cm Diameter Thruster Experiments with Cathode No. 25

1. -Effect of variable aperture baffle

Cathode No. 25 fitted with a variable aperture baffle was installed in the 15-cm diameter permanent magnet geometry thruster. The baffle gave the choice of 4 central apertures of the following geometries:

(i) circular, 1.9 cm diameter, 2.85 cm^2 open area
(ii) annular, 1.9 cm o.d., 1.32 cm^2 open area
(iii) annular, 1.9 cm o.d., 0.61 cm^2 open area
(iv) annular, 1.9 cm o.d., 0.28 cm^2 open area.

and was so designed that both the distance of the baffle from the cathode and the central aperture could be varied during thruster operation.

A series of experiments was then performed on the 15-cm thruster to compare the thruster performance for the different configurations allowed by the four apertures and the main baffle position. The position of the main baffle was varied until the discharge was optimized for a particular central aperture. Table II lists the experimental results, which show that the best performance in terms of both the eV/ion and the mass utilization rate came with the smallest annular aperture, and with the main baffle very close to the thruster end plate. In this situation the annular aperture position corresponds approximately to the edge of the cone (half angle about 30°) of mercury vapor which emanates from the cathode.

Earlier experiments in the 20-cm thruster had indicated that the smallest aperture would give the best performance also in the 15-cm thruster, as was the case, even though the outer diameter of the main baffle was not optimized for the 15-cm diameter thruster. Prior experiments utilizing a baffle without any central aperture have shown that for efficient thruster optimization, some small central aperture is necessary. Such an aperture must profoundly affect the escape of electrons from the cathode environment to the discharge chamber proper, accounting in turn for the change in the source energy per ion.

	Aperture Area cm^2	Source energy/ ion, eV/ion	Mass Utilization, η_m %	Distance of baffle from cathode plate, cm
(i)	2.85	450	77.5	4.0
(ii)	1.32	472	86.7	1.3
(iii)	0.61	450	78.3	0.5
(iv)	0.28	409	84	0.2

TABLE II: 15-cm thruster test results.

In a subsequent experiment, the same cathode was operated with the smallest annular aperture (iv) for a continuous period of 4 hours, while the cathode temperature at the thermocouple junction was maintained at 250°C. The following are the average results

Duration of test	4 hours
Cathode Temperature	250°C
Beam Current	440 mA
Source Energy/ion	417 eV/ion
Mass Utilization, η_m	82%
Electron to Atom Ratio, K_e/K_a	11

which demonstrate satisfactory performance even though the main baffle had not been designed for use with the 15-cm thruster.

2.-Variation of the discharge voltage with magnetic field

While the 15-cm thruster was fitted with Cathode No. 25 and the variable, four aperture baffle, a plot was taken of the discharge voltage as a function of the magnetic field at the mid-point of the thruster axis, for a constant discharge current of 7A. The data (Fig. 22) show that, for a given magnetic field, the aperture size does have a strong effect on the discharge voltage: however for optimum thruster performance (B ~ 34G) the smallest aperture used requires just about the same discharge voltage as the other two annular apertures.

3.-Variation of other thruster parameters with discharge current

With the thruster magnetic field held at 34G, and with the smallest aperture baffle in the optimum position, the discharge current was varied while other thruster parameters were measured. Typically, the results for constant mass flow rate were as follows:

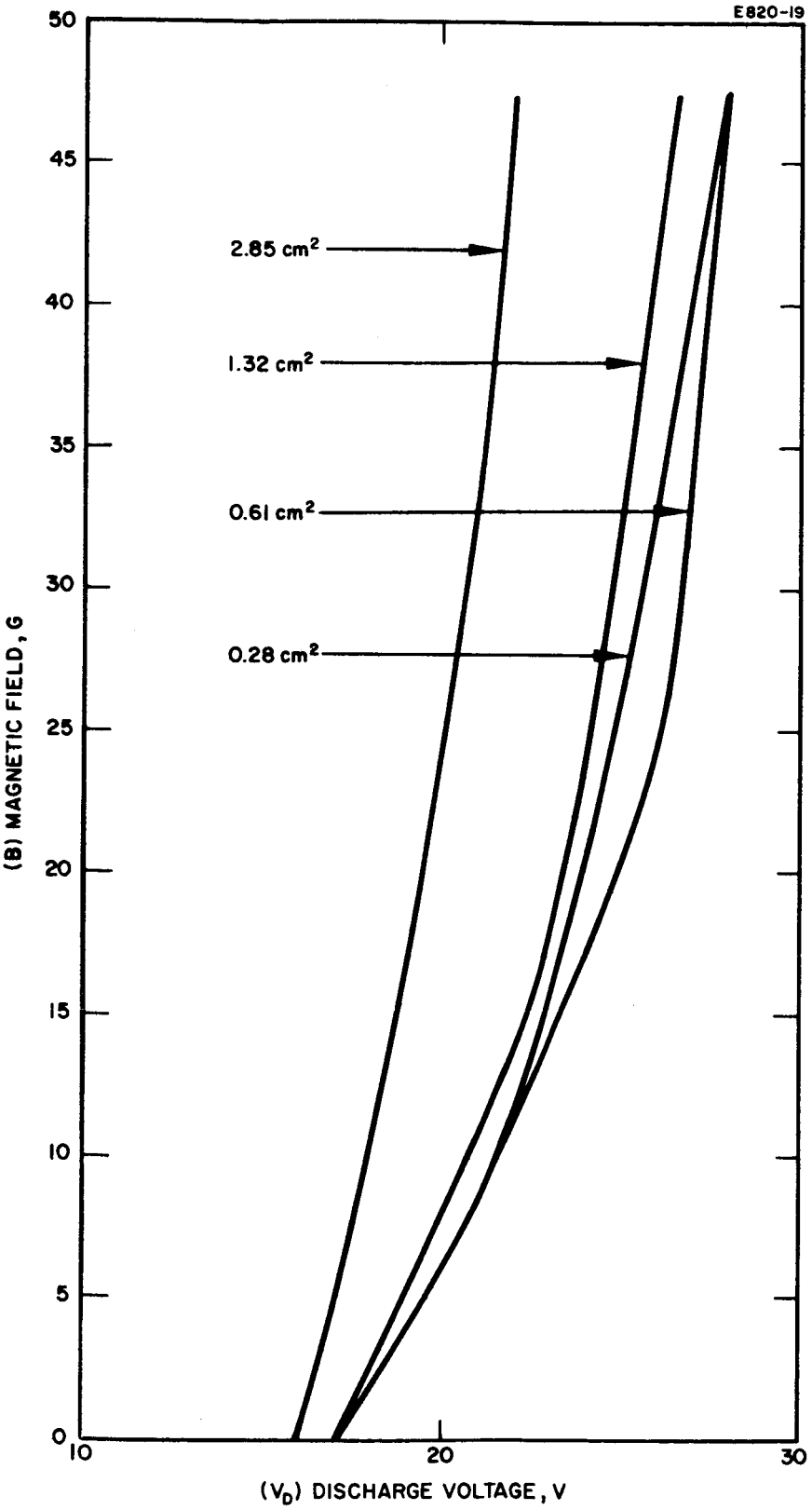

Fig. 22.
Discharge voltage as a function of magnetic field for different aperture areas.

Discharge current I_K, A	Discharge voltage V_D, V	Beam current I_B, mA	Source energy/ion V_S, eV/ion
2	22.0	190	231
3	22.5	260	254
4	23.0	310	310
5	24.0	370	340
6	24.5	405	380
7	25.5	430	415

with a mass utilization of about 80% at the maximum beam current.

These data show an approximately linear dependence of the beam current and the source energy per ion on the discharge current, but exhibit no qualitatively different features when compared with data taken with less effective baffle configurations.

4. Conclusions

The conclusions which can be drawn from the experiments described in the previous sub-sections are the following:

(i) The smallest annular aperture used gave the best thruster performance data, even though the open area of this baffle was only 0.28 cm^2.

(ii) From earlier experiments, completely closing this aperture would reduce the performance.

(iii) Aperture size had an effect on the variation of discharge voltage with thruster magnetic field; however for optimum magnetic field (34G in each case), the superior performance of the smallest aperture cannot be attributed to a change in the discharge voltage.

(iv) The axial baffle position is also critical to good thruster performance.

(v) Even though the main baffle was not designed for the 15-cm thruster, when positioned in an optimum way (close to the cathode) the thruster performance was very satisfactory.

As a result of these experiments, it was decided to examine more closely the contribution of the vapor cone at the cathode to the formation of the ion beam. This is described in the next section.

B. -Discharge Probing Experiments

1. -Experimental

The emphasis during this period has been on an attempt to evaluate the contribution of the vapor cone emerging from the cathode to the production of ions in the discharge. The four-aperture baffle described in the previous section was replaced with a "probing" baffle, the latter having a small (0.6mm diameter) pinhole and a narrow (0.25mm width) slot which could be moved in turn over the central, 1.9 cm diameter circular aperture.

Preliminary experiments have given the data of Table III. When the pinhole is displaced somewhat from the center of the aperture a slight peak is observed in the beam current I_B: this position is such that a line joining the pinhole with the center of the cathode makes an angle of 26° with the cathode centerline. Since vapor is emitted from the cathode in a cone with a half angle of about 30°, this peak is consistent with the existence of a segment of the vapor cone, close to its boundary, which contributes more than the average per unit area to the production of the beam in the discharge chamber.

When the probing hole is moved outside the region of the vapor cone, the beam current falls rapidly to a "background" value which persists even when the central hole in the main baffle is completely covered. This background I_B has been measured at less than 50% of the peak value of I_B, indicating that greater than 50% of the beam current production is caused by the flux of neutrals and/or electrons through the pinhole.

Assuming annular symmetry for the vapor cone, the variation of I_B with slot position can also be used to check the result for the pinhole. Taking into account the geometrical effect as the slot is moved over the central hole, the contribution to I_B per unit area of the vapor cone can be found, and the results are normalized to the pinhole values for comparison. Table III shows that these normalized values peak towards the edge of the vapor cone, and again a rapid decay in I_B as the slot is moved outside of the vapor cone region.

TABLE III

The probing baffle: variation with pinhole or slot position

Distance of pinhole or slot from baffle center, cm	I_B, mA measured for pinhole	I_B, mA for pinhole, less "background"	I_B, mA for the slot, normalized, less "background"
0	400	200	200
0.24	420	220	218
0.48	440	240	300
0.72	350	150	75
0.96 (edge of central hole)	200	0	50
> 1.0	200 ("background")	--	--

2.-Conclusions

It was to be expected that, in the pinhole experiments, confining the pinhole to the vapor cone region would give the greatest I_B. In this situation neutrals and electrons can penetrate to the discharge chamber and join in the ionizing processes there. What is surprising at first sight is that the presence of such a small hole can influence the I_B by such a large amount. It would seem that the hole is too small to greatly influence the efflux of mercury neutrals from the cathode region, so that it principally provides a path for electrons to move to the discharge chamber.

The reason for this can be seen more clearly when it is remembered that the optimum baffle position (for the small aperture, for example, see Section IV) is close to the cathode. Now the aperture is inside or close to the vapor cone and electrons can easily penetrate the small pinhole to escape into the discharge chamber. As the aperture is withdrawn outside the vapor cone, this is a more difficult process for the electrons to accomplish, resulting in a major decrease in the beam current. At the same time, an additional small decrease can be expected because of reduction in neutrals reaching the discharge chamber from feed points close to the axis.

The reason for the slight peak in I_B as the pinhole is moved is not yet understood. It is probably connected with either a non-uniform vapor flux over the solid angle of the cone (this is being investigated under a separate, Company

funded program), or with a non-uniform flux of electrons within the vapor cone, or both.